JOURNAL OF GUIDANCE, CONTROL, AND DYNAMICS
Vol. 31, No. 3, May–June 2008

Flight Dynamics and Hybrid Adaptive Control of Damaged Aircraft

Nhan Nguyen,* Kalmanje Krishnakumar,† and John Kaneshige‡
NASA Ames Research Center,
Moffett Field, California 94035
and
Pascal Nespeca§
University of California, Davis, California 95616

DOI: 10.2514/1.28142

This paper presents a recent study to investigate flight dynamics and adaptive control methods for stability and control recovery of a damaged generic transport aircraft. Aerodynamic modeling of damage effects is performed using an aerodynamic code to assess changes in the stability and control derivatives of the damaged aircraft. Flight dynamics for a general aircraft are developed to account for changes in aerodynamics, mass properties, and the center of gravity that can compromise the stability of the damaged aircraft. An iterative trim analysis is developed to compute incremental trim states. A neural network hybrid direct–indirect adaptive flight control is developed for the stability augmentation control of the damaged aircraft. The proposed method performs an online estimation of damaged plant dynamics to improve the command tracking performance in conjunction with a direct adaptive controller. The plant estimation is based on two approaches: 1) an indirect adaptive law derived from the Lyapunov stability theory to ensure that the tracking error is bounded, and 2) a recursive least-squares method that minimizes the modeling error. Simulations show that the hybrid adaptive controller can provide a significant improvement in the tracking performance over a direct adaptive controller working alone.

Nomenclature

$\mathbf{A}$	=	state matrix for tracking error
$\mathbf{B}$	=	control matrix for tracking error
b	=	wing span
$\mathbf{C}$	=	aerodynamic coefficient matrix, neural network basis functions
C_L, C_D, C_Y	=	lift, drag, and side force coefficients
C_l, C_m, C_n	=	roll, pitch, and yaw moment coefficients
$\bar{c}$	=	mean aerodynamic chord
$\mathbf{e}$	=	tracking error
$\mathbf{F}$	=	force vector
$\mathbf{F}_1, \mathbf{F}_2$	=	state matrices for angular rates and trim states
$\mathbf{G}$	=	control matrix for flight control surfaces
g	=	gravitational acceleration
$\mathbf{H}$	=	angular momentum vector
I	=	inertia scalar
$\mathbf{I}$	=	inertia matrix
J	=	cost function
$\mathbf{K}$	=	gain matrix
L, V	=	Lyapunov candidate functions
L, M, N	=	roll, pitch, and yaw moments
m	=	mass
$\mathbf{P}$	=	Lyapunov matrix
p, q, r	=	roll, pitch, and yaw rates
Q	=	dynamic pressure
$\mathbf{Q}$	=	semipositive-definite matrix
$\mathbf{R}$	=	positive-definite matrix
$\mathbf{r}$	=	position vector
S	=	reference wing area
T	=	engine thrust
u, v, w	=	axial, lateral, and vertical velocity components
$\mathbf{u}_e, \mathbf{u}_{\text{ad}}$	=	pseudocontrol, command augmentation control
$\mathbf{v}$	=	velocity vector
$\mathbf{W}$	=	gravitational force vector, neural network weight matrix
X, Y, Z	=	axial, lateral, and vertical force components
x_0, y_0, z_0	=	coordinates of reference point
$x_e y_e, z_e$	=	coordinates of center of engine thrust
α, β, γ	=	attack, sideslip, and flight path angles
$\boldsymbol{\beta}$	=	neural network basis function
Γ, Γ	=	learning rate, learning rate vector
Δ	=	difference operator
$\boldsymbol{\Delta}$	=	error bound
δ	=	control surface deflection vector
$\delta_a, \delta_e, \delta_r$	=	aileron, elevator, and rudder deflection
$\delta_T, \delta_{\Delta T}$	=	engine throttle and differential throttle positions
$\boldsymbol{\varepsilon}$	=	dynamic inversion error
$\zeta_p, \zeta_q, \zeta_r$	=	reference-model roll, pitch, and yaw damping ratios
$\eta, \vartheta, \lambda, \rho, \varphi, \xi$	=	recursive least-squares parameters
θ, ϕ	=	pitch and bank angles
$\boldsymbol{\theta}, \boldsymbol{\Phi}$	=	input and weight vectors
$\underline{\lambda}$	=	minimum eigenvalue
ρ	=	spectral radius
$\boldsymbol{\sigma}$	=	trim state vector
$\boldsymbol{\omega}, \tilde{\boldsymbol{\omega}}$	=	nonlinear and linearly perturbed angular rate vectors
$\boldsymbol{\omega}_c, \boldsymbol{\omega}_m$	=	angular rate command and reference-model vectors
$\boldsymbol{\omega}_e, \boldsymbol{\omega}_d$	=	angular rate error

Presented as Paper 6049 at the AIAA Guidance, Navigation, and Control Conference, Keystone, CO, 20–24 August 2006; received 2 October 2006; revision received 2 April 2007; accepted for publication 9 April 2007.

*Computer Scientist, Intelligent Systems Division, Mail Stop 269-1. AIAA Senior Member.
†Computer Scientist, Intelligent Systems Division, Mail Stop 269-1. AIAA Associate Fellow.
‡Computer Engineer, Intelligent Systems Division, Mail Stop 269-1.
§Ph.D. Student, Mechanical Aerospace Engineering Department.

$\omega_p, \omega_q, \omega_r$ = reference-model roll, pitch, and yaw frequencies

I. Introduction

AVIATION safety research is concerned with many aspects of safe and reliable operation of today's modern aircraft. Although air travel remains the safest mode of transportation, accidents do occur on rare occasions, which serve as reminders that much work still remains to be done in aviation safety research. American Airlines Flight 587 illustrates the reality of hazards due to structural failures of airframe components that can cause a catastrophic loss of control [1]. Not all structural damages, however, result in a loss of control. The World War II aviation history is filled with many stories of aircraft coming back home safely despite suffering major structural damage to their airframes. An incident involving an Airbus A300-B4 cargo aircraft in 2003 over Baghdad, Iraq further illustrates the ability to maintain controlled flight in the presence of structural damage and hydraulic loss [2]. The Sioux City, Iowa accident involving United Airlines Flight 232 demonstrates that, in certain situations, a limited control authority can be achieved by using the propulsion system to actively control a damaged aircraft [3]. This accident gave an impetus to the propulsion controlled aircraft (PCA) research at NASA [4].

In a damage scenario, some part of a lifting surface may become separated and, as a result, may cause an aircraft's center of gravity (c.g.) to shift unexpectedly. Furthermore, changes in stability and control derivatives associated with changes in aerodynamic characteristics can render a damaged aircraft unstable. Consequently, these effects can lead to a nonequilibrium flight that can adversely affect the ability of a flight control system to maintain aircraft stability. In other instances, reduced structural rigidity of a damaged airframe may manifest in elastic motions that can interfere with a flight control system, and potentially can result in excessive structural loading on critical lifting surfaces. Thus, in a highly dynamic, off-nominal flight environment with many sources of uncertainty caused by damage, a flight control system must be able to cope with complex and uncertain aircraft dynamics.

Numerous effects may be present during a damage situation that can overwhelm a pilot's ability to control an aircraft safety. These effects may include aerodynamic changes, structural degradation, engine damage, reduced flight control effectiveness, the pilot's lack of situational awareness, and others. For example, a structurally impaired aircraft may exhibit unknown aeroservoelastic behaviors that can be difficult to control. Thus, to develop effective adaptive flight control technologies that can be used to retrofit or design a flight control system, an integrated approach is needed that takes into account various interactions among different physical effects, such as aircraft dynamics, airframe structures, engine performance, and flight control actuator dynamics. Research in damage adaptive flight control, therefore, will require various technical disciplines that include physics-based modeling, adaptive flight control, flight planning, and adaptive system verification and validation [5].

Physics-based modeling provides a simulation capability for predicting dynamics of a damaged aircraft and for evaluating adaptive flight control methods. Analytical tools such as computational fluid dynamics, finite element modeling for structural dynamics, flight dynamics, and others will be used to develop this modeling capability. Adaptive flight control is a critical technology that enables a damaged aircraft to maintain stability and maneuverability. Current research in neural network adaptive flight control provides a possibility for developing an effective adaptive flight control system that can adapt to changes in the vehicle stability and control characteristics [6]. Emergency flight planning and postdamage landing technologies are needed to aid a pilot in identifying a suitable landing site, generating in real-time a feasible flight plan within a reduced flight envelope, and ultimately executing a safe landing [7]. Although adaptive flight control has been rigorously investigated, it has not been universally adopted in the aviation industry due to a number of issues associated with verification and validation of adaptive flight control systems. Learning rules for adaptive systems based on the Lyapunov method must be guaranteed to be globally stable under all flight conditions with exogenous disturbances such as turbulence and wind shear. Safety-critical flight software certification through verification and validation of adaptive flight control systems poses a major hurdle that needs further research in the future [8].

This paper focuses on the flight dynamics and adaptive control of a damaged aircraft. The type of damage herein is confined primarily to changes in the aerodynamic configuration of the vehicle brought about by various modes of damage to aerodynamic and flight control surfaces. A flight dynamic model for a generic damaged aircraft is developed to account for various damage scenarios that result in changes to aerodynamics and mass properties. A trim analysis is developed to provide a rapid estimation of new trim states to maintain steady-state flight conditions. Damage adaptive flight control methods are developed to enable a damaged aircraft to maintain stability and command tracking performance. Recent advances in direct adaptive flight control using neural networks provide a foundation for much of this research [9–14]. A hybrid direct–indirect adaptive control method is proposed to extend the current capability of the neural network adaptive flight control. The hybrid adaptive control includes an indirect adaptive law that performs an online estimation of plant dynamics of a damaged aircraft. The stability of this indirect adaptive law is established by the Lyapunov stability theory. An alternative approach is also presented, whereby a recursive least-squares method is used in the plant identification process.

II. Damage Aerodynamic Modeling

A notional twin-engine transport-class aircraft defined by NASA Langley Research Center is used for the study [15]. Figure 1 illustrates this notional aircraft, referred to as a generic transport model (GTM). Understanding the aircraft aerodynamic characteristics during a damage event is critical to developing flight control strategies for a damaged aircraft. Toward that end, aerodynamic modeling is performed using a vortex-lattice code developed at NASA Ames Research Center [16] to estimate the aerodynamic coefficients, and the stability and control derivatives of the damaged GTM for various damage configurations. Aerodynamic characteristics of the damaged GTM are then incorporated into the flight dynamic modeling that will be used to develop adaptive flight control strategies. The damage effects are modeled for separation and penetration damage to lifting surfaces (see Fig. 1). Wing separation damage represents one of the critical modes of damage that is a current focus of this research. Past accidents involving wing separation damage include Pan Am Flight 843 in 1965 that successfully landed and, most recently, Brazil's Gol Flight 1907 in 2006 that was destroyed by in-flight breakup and impact forces due to a midair collision with an Embraer Legacy 600 business jet.

A left wing separation damage can cause a significant loss in the lift capability for the damaged GTM, as shown in Fig. 2. The lift coefficient can be reduced by as much as 25% for a 50% wing loss at $\alpha = 12$ deg and $\beta = 0$ deg. The resulting changes in the lift and pitch moment coefficients can cause the aircraft to be out of trim and thus

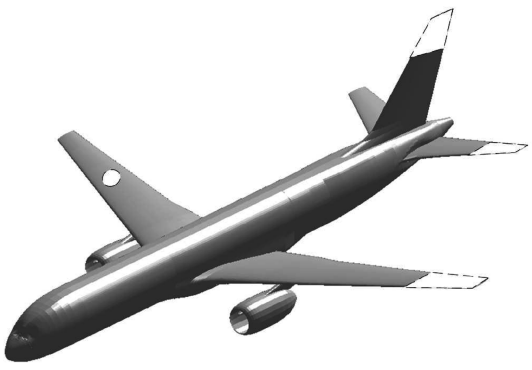

Fig. 1 Generic transport model.

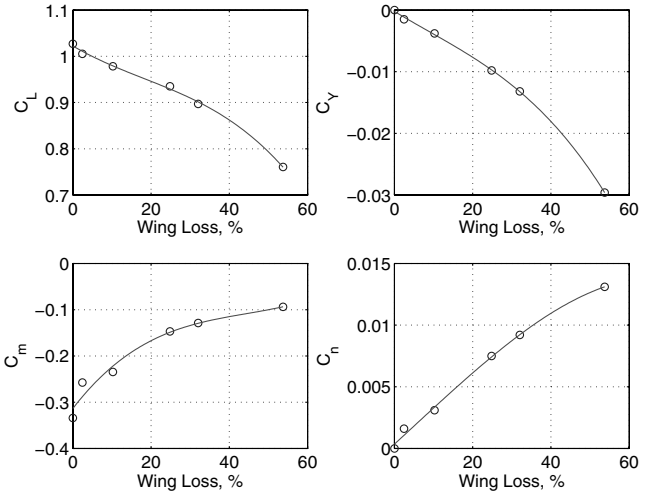

Fig. 2 Aerodynamic coefficients due to left wing separation damage at $\alpha = 12$ deg and $\beta = 0$ deg.

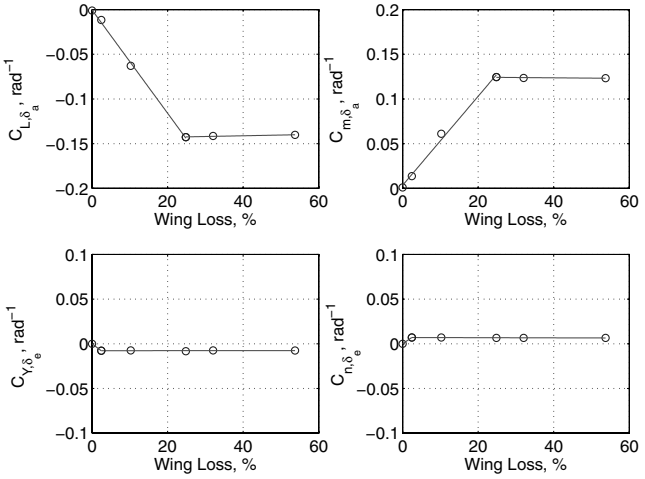

Fig. 3 Control derivatives due to left wing separation damage at $\alpha = 12$ deg and $\beta = 0$ deg.

can adversely affect a flight control system in maintaining a desired airspeed and altitude, unless there is sufficient control power to retrim the aircraft in the pitch axis. In addition, a significant side force and yawing moment can develop without any aileron or rudder input as seen in Fig. 2. Because the longitudinal and lateral motions of the damaged aircraft are coupled together, the damaged aircraft must be retrimmed in all three stability axes simultaneously to maintain a stable flight.

The wing separation damage changes the lift and pitching moment variations caused by the aileron deflections, as shown in Fig. 3. The side force and yawing moment variations with respect to the elevator deflections are negligible, as expected. The abrupt changes in the lift and pitching moment control derivatives are due to a total loss of one of the ailerons for a wing loss that exceeds 25% of the wing span. The consequence of this is that the damaged aircraft would exhibit a pitch-roll coupling. To perform a roll maneuver, the flight control system must compensate for the unwanted pitch motion with the elevators. Similarly, to perform a pitch maneuver, the unwanted roll motion must be compensated for with the ailerons. In light of this, any adaptive flight control strategy must be able to effectively deal with this cross-coupling effect.

III. Flight Dynamics of Damaged Aircraft

An aircraft may develop symmetric damage that causes the c.g. to move in the plane of symmetry or asymmetric damage that causes the c.g. to shift laterally. The movement of the c.g. can compromise the stability of an aircraft. In addition, changes in aerodynamics and

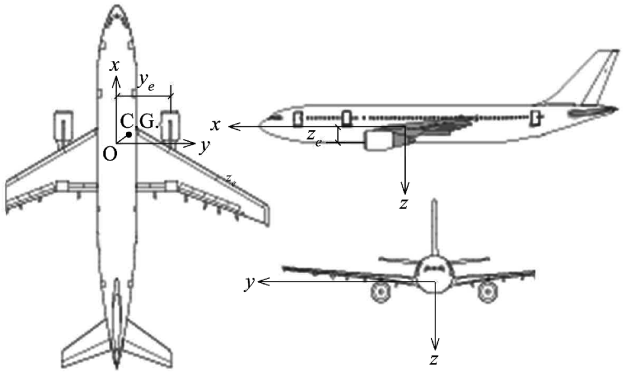

Fig. 4 Center of gravity shift relative to reference point O.

mass properties can also result in a stability problem for a damaged aircraft. The motion of a damaged aircraft, therefore, must be understood to evaluate any flight control design. To this end, we consider an aircraft with a c.g. offset from some reference location, as shown in Fig. 4. The reference location is a fixed point located at the coordinate (x_0, y_0, z_0) on the aircraft, which may be taken as the original c.g. of the undamaged aircraft to maintain the same coordinate reference frame for computing aerodynamic moments. The c.g. of the damaged aircraft can move relative to this fixed reference point.

The damage effect resulting from a left-wing separation damage creates a larger c.g. shift in the lateral direction than in the other two directions, as shown in Fig. 5. This lateral c.g. shift affects the lateral-directional control of the damaged aircraft, more so than the pitch control, due to an additional rolling moment that the flight control system has to compensate for with the available control power.

A. Linear Acceleration

To understand the effect of the c.g. shift, the standard equations of motion for flight dynamics of an aircraft must be modified to allow for this effect. Assuming a flat-earth model for a rigid body aircraft, the force vector in the body-fixed reference frame of the aircraft is

$$\mathbf{F}_B = \frac{\mathrm{d}}{\mathrm{d}t}(m\mathbf{v} + m\boldsymbol{\omega} \times \Delta\mathbf{r}) - \mathbf{W} \tag{1}$$

where $\mathbf{W} = mg[-\sin\theta \quad \cos\theta\sin\phi \quad \cos\theta\cos\phi]^T$ is the gravitational force vector, $\boldsymbol{\omega} = [p \quad q \quad r]^T$ is the aircraft angular rate vector, and $\Delta\mathbf{r} = [\Delta x \quad \Delta y \quad \Delta z]^T$ is the displacement vector from the c.g. to the reference location.

The aircraft mass is assumed to undergo a change so that

$$m = m^* + \Delta m \tag{2}$$

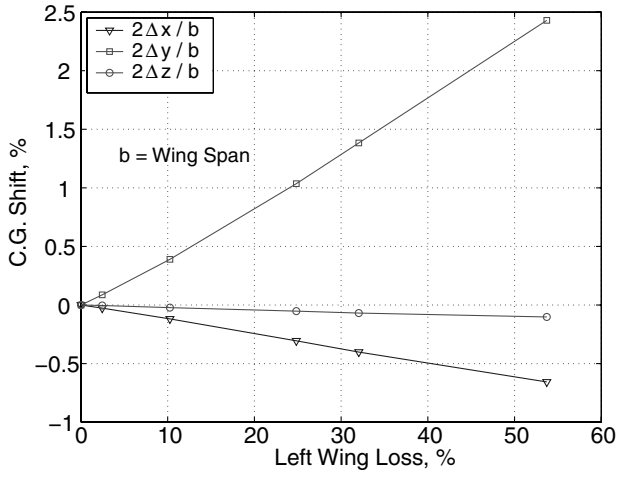

Fig. 5 Center of gravity shift due to left wing separation damage.

where m^* is the original mass of the aircraft and Δm is the negative mass change due to damage.

The force vector then becomes

$$\mathbf{F}_B = m\dot{\mathbf{v}} + m\dot{\boldsymbol{\omega}} \times \Delta\mathbf{r} + m\boldsymbol{\omega} \times \Delta\dot{\mathbf{r}} + \Delta\dot{m}(\mathbf{v} + \boldsymbol{\omega} \times \Delta\mathbf{r}) - \mathbf{W} \tag{3}$$

where the terms $\Delta\dot{\mathbf{r}}$ and $\Delta\dot{m}$ are due to instantaneous changes in the c.g. position and mass, respectively.

If the aircraft experiences a sudden mass loss due to damage, the $\Delta\dot{\mathbf{r}}$ and $\Delta\dot{m}$ terms represent an impulsive force over a short time interval that can be significant and therefore need to be accounted for in simulations. For postdamage flight dynamics, however, the effect of time-varying mass and c.g. position is considered to be small and thus might be neglected. In this study, we are concerned with postdamage flight dynamics and control strategies for a damaged aircraft, and so the effects of sudden changes in the c.g. position and mass are ignored.

Neglecting the impulsive force terms, Eq. (3) is transformed from the body-fixed reference frame to the inertial reference frame as

$$\mathbf{F} = \mathbf{F}_B + m\boldsymbol{\omega} \times (\mathbf{v} + \boldsymbol{\omega} \times \Delta\mathbf{r}) \tag{4}$$

Expanding Eq. (4) gives

$$X = m[\dot{u} - rv + qw - (q^2 + r^2)\Delta x + (pq - \dot{r})\Delta y + (\dot{q} + pr)\Delta z + g\sin\theta] \tag{5}$$

$$Y = m[\dot{v} + ru - pw + (pq + \dot{r})\Delta x - (p^2 + r^2)\Delta y + (qr - \dot{p})\Delta z - g\cos\theta\sin\phi] \tag{6}$$

$$Z = m[\dot{w} - qu + pv + (pr - \dot{q})\Delta x + (qr + \dot{p})\Delta y - (p^2 + q^2)\Delta z - g\cos\theta\cos\phi] \tag{7}$$

The angular acceleration terms appearing in Eqs. (5–7) are a result of the c.g. shift. Thus, the linear acceleration is coupled with the angular acceleration when the c.g. is shifted away from the fixed reference location.

B. Angular Acceleration

We consider the angular momentum vector in the body-fixed reference frame

$$\mathbf{H}_B = \int [\mathbf{r} \times (\boldsymbol{\omega} \times \mathbf{r})]\,\mathrm{d}m + \int (\mathbf{r} \times \mathbf{v})\,\mathrm{d}m \tag{8}$$

Expanding this expression yields

$$\mathbf{H}_B = \mathbf{I}\boldsymbol{\omega} + m\Delta\mathbf{r} \times \mathbf{v} \tag{9}$$

where $\mathbf{I}$ is the inertia matrix with respect to the body-fixed reference frame at the reference location, which can also be expressed as the sum of the original inertia matrix $\mathbf{I}^*$ and the change in the inertia matrix $\Delta\mathbf{I}$ due to damage

$$\mathbf{I} = \mathbf{I}^* + \Delta\mathbf{I} \tag{10}$$

The time rate of change in the angular momentum gives rise to the following moment equation in the inertial reference frame

$$\mathbf{M} = \frac{\mathrm{d}\mathbf{H}_B}{\mathrm{d}t} + \boldsymbol{\omega} \times \mathbf{H}_B = \mathbf{I}\dot{\boldsymbol{\omega}} + \Delta\dot{\mathbf{I}}\boldsymbol{\omega} + m\Delta\mathbf{r} \times \dot{\mathbf{v}} + m\Delta\dot{\mathbf{r}} \times \mathbf{v} + \Delta\dot{m}\Delta\mathbf{r} \times \mathbf{v} + \boldsymbol{\omega} \times \mathbf{I}\boldsymbol{\omega} + m\boldsymbol{\omega} \times (\Delta\mathbf{r} \times \mathbf{v}) \tag{11}$$

Neglecting terms due to time-varying mass, inertia, and c.g. position, Eq. (11) can be expanded into the following moment equations:

$$L = I_{xx}\dot{p} - I_{xy}\dot{q} - I_{xz}\dot{r} + I_{xy}pr - I_{xz}pq + (I_{zz} - I_{yy})qr + I_{yz}(r^2 - q^2) + m(qv + rw)\Delta x + m(\dot{w} - qu)\Delta y - m(\dot{v} + ru)\Delta z \tag{12}$$

$$M = -I_{xy}\dot{p} + I_{yy}\dot{q} - I_{yz}\dot{r} + I_{yz}pq - I_{xy}qr + (I_{xx} - I_{zz})pr + I_{xz}(p^2 - r^2) - m(\dot{w} + pv)\Delta x + m(pu + rw)\Delta y + m(\dot{u} - rv)\Delta z \tag{13}$$

$$N = -I_{xz}\dot{p} - I_{yz}\dot{q} + I_{zz}\dot{r} + I_{xz}qr - I_{yz}pr + (I_{yy} - I_{xx})pq + I_{xy}(q^2 - p^2) + m(\dot{v} - pw)\Delta x - m(\dot{u} + qw)\Delta y + m(pu + qv)\Delta z \tag{14}$$

Equations (12–14) indicate that the c.g. offset effectively creates additional moments for which a flight control system has to compensate.

C. Aerodynamic and Propulsive Forces and Moments

Assuming that the engine thrust vector is aligned with the x axis of the aircraft, then the forces and moments due to aerodynamics and the propulsion are

$$X = \delta_T T_{\max} + (C_L^* + \Delta C_L)QS\sin\alpha - (C_D^* + \Delta C_D)QS\cos\alpha\cos\beta \tag{15}$$

$$Y = (C_Y^* + \Delta C_Y)QS - (C_D^* + \Delta C_D)QS\sin\beta \tag{16}$$

$$Z = -(C_L^* + \Delta C_L)QS\cos\alpha - (C_D^* + \Delta C_D)QS\sin\alpha\cos\beta \tag{17}$$

$$L = (C_l^* + \Delta C_l)QSb \tag{18}$$

$$M = (C_m^* + \Delta C_m)QS\bar{c} + \delta_T T_{\max}(z_e - z_0) \tag{19}$$

$$N = (C_n^* + \Delta C_n)QSb + \delta_{\Delta T} T_{\max} y_e + \delta_T T_{\max} y_0 \tag{20}$$

where $(x_e, \pm y_e, z_e)$ are the centers of the right (+) and left (−) engine thrust vectors, and the superscript * denotes the force and moment coefficients for the undamaged aircraft evaluated at the reference location.

We assume that the left and right engines produce a combined maximum thrust equal to $T_{\max}$ and are symmetrically positioned with respect to the aircraft fuselage reference line. Then δ_T, where $0 \le \delta_T \le 1$, is the throttle position corresponding to a desired total engine thrust, and $\delta_{\Delta T}$, where $-1/2 \le \delta_{\Delta T} \le 1/2$, is the throttle differential position that results in a desired engine differential thrust equal to the left engine thrust minus the right engine thrust. The incremental changes in the aerodynamic coefficients due to damage are defined as

$$\Delta\mathbf{C} = \Delta\mathbf{C}_0 + \Delta\mathbf{C}_\alpha\alpha + \Delta\mathbf{C}_\beta\beta + \Delta\mathbf{C}_{\boldsymbol{\delta}}\boldsymbol{\delta} + \Delta\mathbf{C}_{\boldsymbol{\omega}}\boldsymbol{\omega} \tag{21}$$

where

$$\Delta\mathbf{C} = [C_L - C_L^* \quad C_D - C_D^* \quad C_Y - C_Y^* \quad C_l - C_l^* \quad C_m - C_m^* \quad C_n - C_n^*]^T$$

$\boldsymbol{\delta} = [\delta_a \quad \delta_e \quad \delta_r]^T$ is the flight control surface deflection vector, the subscripts α, β, $\boldsymbol{\delta}$, and $\boldsymbol{\omega}$ denote the derivatives, and the subscript zero denotes the coefficients at $\alpha = 0$ and $\beta = 0$.

The last term in Eq. (21) is the damping term due to the angular rate of the aircraft. This term can significantly affect the aircraft short-period and dutch roll modes.

IV. Trim Analysis

The aerodynamic forces on an asymmetric aircraft due to a lateral c.g. shift include a nonzero side force component that is generally not experienced on a symmetric aircraft. For a steady flight, the side force equation becomes

$$mg\cos\theta\sin\phi + (C_Y^* + \Delta C_Y)QS - (C_D^* + \Delta C_D)QS\sin\beta = 0 \tag{22}$$

The side force equilibrium for an asymmetric aircraft can be accomplished by trimming the aircraft at a nonzero bank angle ϕ with a zero sideslip angle β. However, this would result in a limitation in the bank angle in coordinated turn maneuvers. Another side force trim approach is to trim the aircraft level with a zero bank angle ϕ but at a nonzero sideslip angle β. In either case, the aircraft would have to be trimmed in both the longitudinal and lateral directions simultaneously by searching for the steady-state solution of Eqs. (15–17) with $\phi = 0$ or $\beta = 0$. The trim analysis thus computes the trim values for the angle of attack α, bank angle ϕ, or sideslip angle β, and engine throttle position δ_T, as functions of the aileron deflection δ_a, elevator deflection δ_e, and rudder deflection δ_r for a given aircraft Mach number and altitude. We assume that the engine thrusts will be symmetric at all times so that $\delta_{\Delta T} = 0$.

If an undamaged aircraft has a mass m^* and is flying wing-level, i.e., $\phi^* = 0$, with no control input at the original trim angle of attack α^*, sideslip angle $\beta^* = 0$, and trim throttle position δ_T^* corresponding to a lift coefficient C_L^*, drag coefficient C_D^*, and side force coefficient $C_Y^* = 0$, then for small changes in the aircraft mass and aerodynamic coefficients, we can determine the incremental trim angle of attack, bank angle, and throttle position to maintain approximately the same trim airspeed V and flight path angle γ^*, by taking small but finite differences of Eqs. (15–17) and setting them to zero as follows:

$$\begin{aligned}
&\Delta\delta_T T_{\max} + (\Delta C_L + C_{L,\alpha}\Delta\alpha + C_{L,\beta}\Delta\beta + C_{L,\boldsymbol{\delta}}\boldsymbol{\delta})QS\sin\alpha^* \\
&\quad + (C_L + C_{L,\alpha}\Delta\alpha + C_{L,\beta}\Delta\beta + C_{L,\boldsymbol{\delta}}\boldsymbol{\delta})QS\cos\alpha^*\Delta\alpha \\
&\quad - (\Delta C_D + C_{D,\alpha}\Delta\alpha + C_{D,\beta}\Delta\beta + C_{D,\boldsymbol{\delta}}\boldsymbol{\delta})QS\cos\alpha^* \\
&\quad + (C_D + C_{D,\alpha}\Delta\alpha + C_{D,\beta}\Delta\beta + C_{D,\boldsymbol{\delta}}\boldsymbol{\delta})QS\sin\alpha^*\Delta\alpha \\
&\quad - mg\cos(\gamma^* + \alpha^*)\Delta\alpha - \Delta mg\sin(\gamma^* + \alpha^*) = 0
\end{aligned} \tag{23}$$

$$\begin{aligned}
&(\Delta C_Y + C_{Y,\alpha}\Delta\alpha + C_{Y,\beta}\Delta\beta + C_{Y,\boldsymbol{\delta}}\boldsymbol{\delta})QS - (C_D + C_{D,\alpha}\Delta\alpha \\
&\quad + C_{D,\beta}\Delta\beta + C_{D,\boldsymbol{\delta}}\boldsymbol{\delta})QS\Delta\beta + mg[\cos(\gamma^* + \alpha^*) \\
&\quad - \sin(\gamma^* + \alpha^*)\Delta\alpha]\Delta\phi = 0
\end{aligned} \tag{24}$$

$$\begin{aligned}
&-(\Delta C_L + C_{L,\alpha}\Delta\alpha + C_{L,\beta}\Delta\beta + C_{L,\boldsymbol{\delta}}\boldsymbol{\delta})QS\cos\alpha^* \\
&\quad + (C_L + C_{L,\alpha}\Delta\alpha + C_{L,\beta}\Delta\beta + C_{L,\boldsymbol{\delta}}\boldsymbol{\delta})QS\sin\alpha^*\Delta\alpha \\
&\quad - (\Delta C_D + C_{D,\alpha}\Delta\alpha + C_{D,\beta}\Delta\beta + C_{D,\boldsymbol{\delta}}\boldsymbol{\delta})QS\sin\alpha^* \\
&\quad - (C_D + C_{D,\alpha}\Delta\alpha + C_{D,\beta}\Delta\beta + C_{D,\boldsymbol{\delta}}\boldsymbol{\delta})QS\cos\alpha^*\Delta\alpha \\
&\quad - mg\sin(\gamma^* + \alpha^*)\Delta\alpha + \Delta mg\cos(\gamma^* + \alpha^*) = 0
\end{aligned} \tag{25}$$

To find the trim bank angle at a zero sideslip angle, we set $\Delta\beta = 0$ in the preceding equations. Equation (25), then, is a quadratic equation in terms of $\Delta\alpha$ whose solution can easily be computed as

$$\Delta\alpha = -\frac{b}{2a} + \sqrt{\left(\frac{b}{2a}\right)^2 - \frac{c}{a}} \tag{26}$$

with

$$a = (C_{L,\alpha}\sin\alpha^* - C_{D,\alpha}\cos\alpha^*)QS \tag{27}$$

$$\begin{aligned}
b = &[(C_L + C_{L,\boldsymbol{\delta}}\boldsymbol{\delta} - C_{D,\alpha})\sin\alpha^* - (C_D + C_{D,\boldsymbol{\delta}}\boldsymbol{\delta} \\
&+ C_{L,\alpha})\cos\alpha^*]QS - mg\sin(\gamma^* + \alpha^*)
\end{aligned} \tag{28}$$

$$\begin{aligned}
c = &-[(\Delta C_L + C_{L,\boldsymbol{\delta}}\boldsymbol{\delta})\cos\alpha^* + (\Delta C_D + C_{D,\boldsymbol{\delta}}\boldsymbol{\delta})\sin\alpha^*]QS \\
&+ \Delta mg\cos(\gamma^* + \alpha^*)
\end{aligned} \tag{29}$$

From Eq. (24), we now find the trim bank angle

$$\Delta\phi = \frac{-(\Delta C_Y + C_{Y,\alpha}\Delta\alpha + C_{Y,\boldsymbol{\delta}}\boldsymbol{\delta})QS}{mg[\cos(\gamma^* + \alpha^*) - \sin(\gamma^* + \alpha^*)\Delta\alpha]} \tag{30}$$

Finally, the incremental trim throttle position can be solved directly from Eq. (23).

Trimming the damaged aircraft with the bank angle will result in a reduced bank angle limit. This would potentially affect the aircraft's turn capability. Moreover, the aircraft will not fly wings level, which would not be acceptable for a landing approach. Therefore, the damaged aircraft can be trimmed alternatively with the sideslip angle. This will enable the aircraft to maintain a level flight, but the control authority of the rudder control surface will be reduced because it has to compensate for the nonzero sideslip angle. To obtain the trim sideslip angle, we set $\Delta\phi = 0$ in Eq. (24) and solve Eqs. (23–25) simultaneously for $\Delta\delta_T$, $\Delta\alpha$, and $\Delta\phi$ or $\Delta\beta$.

In examining Eq. (24) with $\Delta\phi = 0$, it is noted that if the undamaged aircraft is in a cruise phase at a minimum drag, then the trim sideslip angle for the damaged aircraft could be large if the damage develops a significant side force. Typically, it is not advisable to fly the aircraft at a high sideslip angle because of stability concerns. Depending on the extent of damage, an effective trim approach may be one that uses a combination of the trim bank angle and sideslip angle.

The trim analysis shows that the damaged aircraft would have to be retrimmed with a new trim angle of attack $\alpha = \alpha^* + \Delta\alpha$, bank angle $\phi = \Delta\phi$, or sideslip angle $\beta = \Delta\beta$, and throttle position $\delta_T = \delta_T^* + \Delta\delta_T$, to achieve an equilibrium flight. The trim α, ϕ, or β, and δ_T are all functions of the flight control surface deflection $\boldsymbol{\delta}$ as well as the aircraft damage configuration. In general, the stability and control derivatives needed to retrim the damaged aircraft are not known. Assuming that the effect of damage on the aerodynamics can be estimated, a trim calculation strategy is to initially retrim the damaged aircraft with a zero control surface deflection by setting $\boldsymbol{\delta} = \mathbf{0}$ in Eqs. (23–25). Then, using the inner-loop rate-command-attitude-hold (RCAH) control, new control surface deflections for the damaged aircraft can be obtained. This allows the trim values to be recomputed until the final trim state is obtained.

V. Damage Adaptive Flight Control

Most conventional flight control systems use extensive gain-scheduling to achieve desired handling qualities. Although this approach has proven to be very successful, the development process can be expensive and often results in aircraft-specific implementations. Over the past several years, various adaptive flight control techniques have been investigated [9–14,17–19]. A damaged aircraft can pose a significant challenge to a conventional flight control system because the damaged aircraft dynamics may deviate from its design characteristics substantially, thereby causing a degraded performance of the flight control system. This makes it difficult for a conventional flight control system to cope with changes in the stability and control characteristics of the damaged aircraft. Adaptive flight control provides a possibility for maintaining the stability of a damaged aircraft by being able to adapt to system uncertainties. Research in adaptive control has spanned several decades, but challenges in obtaining robustness in the presence of unmodeled dynamics, parameter uncertainties, and disturbances, as well as the ongoing concerns with verification and validation, still remain [17]. Adaptive control laws may be divided into direct and indirect approaches. Indirect adaptive control methods are based on identification of unknown plant parameters and certainty-equivalence control schemes derived from the parameter estimates which are assumed to be their true values [20]. Parameter identification techniques, such as recursive least-squares and neural networks, have been used in indirect adaptive control methods [18].

In contrast, direct adaptive control methods directly adjust control parameters to account for system uncertainties without identifying unknown plant parameters explicitly. In recent years, model-reference direct adaptive control using neural networks has been a topic of great research interest [10–14,19]. In particular, Rysdyk and Calise described a method for augmenting acceleration commands via a neural network direct adaptive control law to improve handling qualities [10]. Johnson et al. introduced a pseudocontrol hedging approach for dealing with control input characteristics such as actuator saturation, rate limit, and linear input dynamics [19]. Idan et al. studied a hierarchical neural network adaptive control using secondary actuators such as engine propulsion to accommodate for failures of primary actuators [12]. Hovakimyan et al. developed an output feedback adaptive control to address parametric uncertainty and unmodeled dynamics [14]. Lyapunov stability theory is an indispensable tool which has been used to establish stable and robust adaptive laws for these adaptive control methods.

In the current research, we first adopt the work by Rysdyk and Calise [10] to develop a neural network direct adaptive flight control with a dynamic inversion controller for a damaged aircraft. The adaptive flight control is able to provide consistent handling qualities without requiring extensive gain-scheduling or explicit system identification of the damaged aircraft dynamics. This particular architecture uses pretrained and online learning neural networks and a reference model to specify desired handling qualities. Pretrained neural networks are used to provide estimates of aerodynamic stability and control characteristics required for the model inversion. Online learning neural networks are used to compensate for errors and adapt to changes in the aircraft dynamics. As a result, consistent handling qualities may be achieved across flight conditions and for different damage configurations. An architecture of the neural network direct adaptive flight control is shown in Fig. 6. We will extend this architecture to include an indirect adaptive control approach that provides an online estimation of the true plant dynamics. The estimation of the damaged plant dynamics is provided by an indirect adaptive law based on the Lyapunov stability analysis. As an alternate approach, we also consider a recursive least-squares method for performing the online estimation.

A. Linearized Plant Dynamics

First, we need to arrive at a set of small perturbation equations in terms of the angular accelerations for designing a feedback linearization control. To maintain a desired airspeed and altitude, the damaged aircraft has to be retrimmed using the aforementioned trim method. The damaged aircraft stability must be augmented by the RCAH controller. This results in control surface deflections necessary to maintain a desired angular rate command. Toward that end, we eliminate the linear accelerations from Eqs. (12–14) by combining them with Eqs. (5–7). The resulting nonlinear equations in terms of the angular accelerations are

$$\begin{aligned}&\bar{I}_{xx}\dot{p}-\bar{I}_{xy}\dot{q}-\bar{I}_{xz}\dot{r}+\bar{I}_{xy}pr-\bar{I}_{xz}pq+(\bar{I}_{zz}-\bar{I}_{yy})qr\\&\quad+\bar{I}_{yz}(r^2-q^2)+m(qv+rw)\Delta x-mpv\Delta y-mpw\Delta z\\&\quad=(C_l^*+\Delta\bar{C}_l)QSb\end{aligned}\tag{31}$$

$$\begin{aligned}&-\bar{I}_{xy}\dot{p}+\bar{I}_{yy}\dot{q}-\bar{I}_{yz}\dot{r}+\bar{I}_{yz}pq-\bar{I}_{xy}qr+(\bar{I}_{xx}-\bar{I}_{zz})pr\\&\quad+\bar{I}_{xz}(p^2-r^2)-mqu\Delta x+m(pu+rw)\Delta y-mqw\Delta z\\&\quad=(C_m^*+\Delta\bar{C}_m)QS\bar{c}+\delta_T T_{\max}(z_e-z_0)\end{aligned}\tag{32}$$

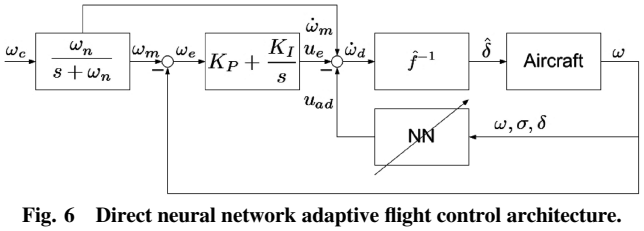

Fig. 6 Direct neural network adaptive flight control architecture.

$$\begin{aligned}&-\bar{I}_{xz}\dot{p}-\bar{I}_{yz}\dot{q}+\bar{I}_{zz}\dot{r}+\bar{I}_{xz}qr-\bar{I}_{yz}pr+(\bar{I}_{yy}-\bar{I}_{xx})pq\\&\quad+\bar{I}_{xy}(q^2-p^2)-mru\Delta x-mrv\Delta y+m(pu+qv)\Delta z\\&\quad=(C_n^*+\Delta\bar{C}_n)QSb+\delta_T T_{\max}y_0\end{aligned}\tag{33}$$

with

$$\begin{aligned}\Delta\bar{C}_l&=\Delta C_l+C_y\frac{\Delta z}{b}-C_z\frac{\Delta y}{b}\\&\quad-\frac{mg}{QS}\left(\cos\theta\cos\phi\frac{\Delta y}{b}-\cos\theta\sin\phi\frac{\Delta z}{b}\right)\end{aligned}\tag{34}$$

$$\begin{aligned}\Delta\bar{C}_m&=\Delta C_m-C_x\frac{\Delta z}{\bar{c}}+C_z\frac{\Delta x}{\bar{c}}\\&\quad+\frac{mg}{QS}\left(\cos\theta\cos\phi\frac{\Delta x}{\bar{c}}+\sin\theta\frac{\Delta z}{\bar{c}}\right)\end{aligned}\tag{35}$$

$$\begin{aligned}\Delta\bar{C}_n&=\Delta C_n+C_x\frac{\Delta y}{b}-C_y\frac{\Delta x}{b}\\&\quad-\frac{mg}{QS}\left(\cos\theta\sin\phi\frac{\Delta x}{b}+\sin\theta\frac{\Delta y}{b}\right)\end{aligned}\tag{36}$$

where C_x, C_y, and C_z are X-, Y-, and Z-force coefficients normalized to the dynamic pressure loading QS.

The linear dynamics of the damaged aircraft are then computed by linearizing Eqs. (31–33)

$$(\bar{\mathbf{I}}^*+\Delta\bar{\mathbf{I}})\dot{\tilde{\boldsymbol{\omega}}}=(\mathbf{f}_1^*+\Delta\mathbf{f}_1)\tilde{\boldsymbol{\omega}}+(\mathbf{f}_2^*+\Delta\mathbf{f}_2)\boldsymbol{\sigma}+(\mathbf{g}^*+\Delta\mathbf{g})\boldsymbol{\delta}\tag{37}$$

where $\tilde{\boldsymbol{\omega}}=[\,\Delta p\quad \Delta q\quad \Delta r\,]^T$ is the angular rate vector, $\boldsymbol{\sigma}=[\,\Delta\alpha\quad \Delta\beta\quad \Delta\phi\quad \Delta\delta_T\,]^T$ is the trim parameter vector, and

$$\mathbf{f}_1^*=QS\begin{bmatrix}C_{l,p}^*b & C_{l,q}^*b & C_{l,r}^*b\\ C_{m,p}^*\bar{c} & C_{m,q}^*\bar{c} & C_{m,r}^*\bar{c}\\ C_{n,p}^*b & C_{n,q}^*b & C_{n,r}^*b\end{bmatrix}$$

$$\begin{aligned}\Delta\mathbf{f}_1&=QS\begin{bmatrix}\Delta\bar{C}_{l,p}b & \Delta\bar{C}_{l,q}b & \Delta\bar{C}_{l,r}b\\ \Delta\bar{C}_{m,p}\bar{c} & \Delta\bar{C}_{m,q}\bar{c} & \Delta\bar{C}_{m,r}\bar{c}\\ \Delta\bar{C}_{n,p}b & \Delta\bar{C}_{n,q}b & \Delta\bar{C}_{n,r}b\end{bmatrix}\\&\quad+m\begin{bmatrix}v\Delta y+w\Delta z & -v\Delta x & -w\Delta x\\ -u\Delta y & u\Delta x+w\Delta z & -w\Delta y\\ -u\Delta z & -v\Delta z & u\Delta x+v\Delta y\end{bmatrix}\end{aligned}$$

$$\begin{aligned}\mathbf{f}_2^*&=QS\begin{bmatrix}C_{l,\alpha}^*b & C_{l,\beta}^*b & 0 & 0\\ C_{m,\alpha}^*\bar{c}+\frac{\delta_T T_{\max,\alpha}(z_e-z_0)}{QS} & C_{m,\beta}^*\bar{c}+\frac{\delta_T T_{\max,\beta}(z_e-z_0)}{QS} & 0 & \frac{T_{\max}(z_e-z_0)}{QS}\\ C_{n,\alpha}^*b+\frac{\delta_T T_{\max,\alpha}y_0}{QS} & C_{n,\beta}^*b+\frac{\delta_T T_{max,\beta}y_0}{QS} & 0 & \frac{T_{\max}y_0}{QS}\end{bmatrix}\\\Delta\mathbf{f}_2&=QS\begin{bmatrix}\Delta\bar{C}_{l,\alpha}b & \Delta\bar{C}_{l,\beta}b & \Delta\bar{C}_{l,\phi}b & \Delta\bar{C}_{l,\delta_T}b\\ \Delta\bar{C}_{m,\alpha}\bar{c} & \Delta\bar{C}_{m,\beta}\bar{c} & \Delta\bar{C}_{m,\phi}\bar{c} & \Delta\bar{C}_{m,\delta_T}\bar{c}\\ \Delta\bar{C}_{n,\alpha}b & \Delta\bar{C}_{n,\beta}b & \Delta\bar{C}_{n,\phi}b & \Delta C_{n,\delta_T b}\end{bmatrix}\end{aligned}$$

$$\begin{aligned}\mathbf{g}^*&=QS\begin{bmatrix}C_{l,\delta_a}^*b & C_{l,\delta_e}^*b & C_{l,\delta_r}^*b\\ C_{m,\delta_a}^*\bar{c} & C_{m,\delta_e}^*\bar{c} & C_{m,\delta_r}^*\bar{c}\\ C_{n,\delta_a}^*b & C_{n,\delta_e}^*b & C_{n,\delta_r}^*b\end{bmatrix}\\\Delta\mathbf{g}&=QS\begin{bmatrix}\Delta\bar{C}_{l,\delta_a}b & \Delta\bar{C}_{l,\delta_e}b & \Delta\bar{C}_{l,\delta_r}b\\ \Delta\bar{C}_{m,\delta_a}\bar{c} & \Delta\bar{C}_{m,\delta_e}\bar{c} & \Delta\bar{C}_{m,\delta_r}\bar{c}\\ \Delta\bar{C}_{n,\delta_a}b & \Delta\bar{C}_{n,\delta_e}b & \Delta\bar{C}_{n,\delta_r}b\end{bmatrix}\end{aligned}$$

Equation (37) is the linear perturbation equation for the angular acceleration of a damaged aircraft which can also be written in a state-space form as

$$\dot{\tilde{\boldsymbol{\omega}}} = (\mathbf{F}_1 + \Delta\mathbf{F}_1)\tilde{\boldsymbol{\omega}} + (\mathbf{F}_2 + \Delta\mathbf{F}_2)\boldsymbol{\sigma} + (\mathbf{G} + \Delta\mathbf{G})\boldsymbol{\delta} \tag{38}$$

where $\mathbf{F}_1 = \bar{\mathbf{I}}^{*-1}\mathbf{f}_1^*$, $\mathbf{F}_2 = \bar{\mathbf{I}}^{*-1}\mathbf{f}_2^*$, $\mathbf{G} = \bar{\mathbf{I}}^{*-1}\mathbf{g}^*$, $\Delta\mathbf{F}_1 = \bar{\mathbf{I}}^{-1}(\mathbf{f}_1^* + \Delta\mathbf{f}_1) - \mathbf{F}_1$, $\Delta\mathbf{F}_2 = \bar{\mathbf{I}}^{-1}(\mathbf{f}_2^* + \Delta\mathbf{f}_2) - \mathbf{F}_2$, and $\Delta\mathbf{G} = \bar{\mathbf{I}}^{-1}(\mathbf{g}^* + \Delta\mathbf{g}) - \mathbf{G}$.

Under ideal situations, the plant dynamics of an undamaged aircraft are assumed to be known. Upon a damage occurrence, the plant dynamics become uncertain. As a result, the stability and control derivative matrices $\Delta\mathbf{F}_1$, $\Delta\mathbf{F}_2$, and $\Delta\mathbf{G}$ are usually unknown. Consequently, a flight control system needs to be able to adapt to the uncertain plant dynamics of the damaged aircraft. The angular acceleration vector $\dot{\tilde{\boldsymbol{\omega}}}$ of the damaged aircraft may be written as the sum of an ideal angular acceleration vector $\dot{\boldsymbol{\omega}}_i$ of the undamaged aircraft and a differential angular acceleration vector $\Delta\dot{\boldsymbol{\omega}}$ due to damage

$$\dot{\tilde{\boldsymbol{\omega}}} = \dot{\boldsymbol{\omega}}_i + \Delta\dot{\boldsymbol{\omega}} \tag{39}$$

The ideal, undamaged aircraft plant dynamics can be written as

$$\dot{\boldsymbol{\omega}}_i = \mathbf{F}_1\tilde{\boldsymbol{\omega}} + \mathbf{F}_2\boldsymbol{\sigma} + \mathbf{G}\boldsymbol{\delta} \tag{40}$$

where the stability and control matrices for the undamaged aircraft $\mathbf{F}_1$, $\mathbf{F}_2$, and $\mathbf{G}$ are assumed to be known.

B. Neural Network Direct Adaptive Control

The goal of the adaptive flight control is to be able to fly a damaged aircraft whose handling characteristics are specified by a reference model. The control adaptation must be able to accommodate damage using the available flight control surfaces. A reference model is used to filter a rate command vector $\boldsymbol{\omega}_c$ into a reference angular rate vector $\boldsymbol{\omega}_m$ and a reference angular acceleration vector $\dot{\boldsymbol{\omega}}_m$ via a first-order model

$$\dot{\boldsymbol{\omega}}_m + \boldsymbol{\omega}_n\boldsymbol{\omega}_m = \boldsymbol{\omega}_n\boldsymbol{\omega}_c \tag{41}$$

where $\boldsymbol{\omega}_n = \mathrm{diag}(\omega_p, \omega_q, \omega_r)$ is the reference-model frequency matrix.

The reference-model frequencies must be chosen appropriately to obtain a good transient response that satisfies position and rate limits on the control surface deflections. For transport aircraft, typical values of ω_p, ω_q, and ω_r are 3.5, 2.5, and 2.0, respectively [6]. In cases when the reference model is over- or underspecified, these parameters must be adjusted accordingly. The tuning of the reference-model parameters can be performed using an adaptive-critic approach to ensure that the flight control can track the reference model to achieve desired handling qualities [21].

The reference-model angular rate vector $\boldsymbol{\omega}_m$ is compared with the actual angular rate output $\tilde{\boldsymbol{\omega}}$ to form a tracking error signal $\boldsymbol{\omega}_e = \boldsymbol{\omega}_m - \tilde{\boldsymbol{\omega}}$. A pseudocontrol vector $\mathbf{u}_e$ is constructed using a proportional-integral (PI) feedback scheme to better handle errors detected from the roll rate, pitch rate, and yaw rate feedback. The error dynamics, defined by proportional and integral gains, must be fast enough to track the reference model, yet slow enough to not interfere with actuator dynamics. A windup protection is designed to limit the integrator at its current value when a control surface is commanded beyond its limit. The pseudocontrol vector $\mathbf{u}_e$ is computed as

$$\mathbf{u}_e = \mathbf{K}_P\boldsymbol{\omega}_e + \mathbf{K}_I\int_0^t \boldsymbol{\omega}_e\,\mathrm{d}\tau \tag{42}$$

To maintain a reasonable tracking performance and loop gains, it is found that the proportional and integral gains can be selected to achieve second-order error dynamics with natural frequencies that match the reference-model frequencies and damping ratios of $\zeta_p = \zeta_q = \zeta_r = 1/\sqrt{2}$ according to

$$\mathbf{K}_P = \mathrm{diag}(2\zeta_p\omega_p, 2\zeta_q\omega_q, 2\zeta_r\omega_r) \tag{43}$$

$$\mathbf{K}_I = \mathrm{diag}(\omega_p^2, \omega_q^2, \omega_r^2) \tag{44}$$

A dynamic inversion controller is computed to obtain an estimated control surface deflection command $\hat{\boldsymbol{\delta}}$ to achieve a desired angular acceleration vector $\dot{\boldsymbol{\omega}}_d$ using the known plant dynamics of the undamaged aircraft from Eq. (40):

$$\hat{\boldsymbol{\delta}} = \mathbf{G}^{-1}(\dot{\boldsymbol{\omega}}_d - \mathbf{F}_1\tilde{\boldsymbol{\omega}} - \mathbf{F}_2\boldsymbol{\sigma}) \tag{45}$$

assuming that $\mathbf{G}$ is invertible.

Because the true plant dynamics of the damaged aircraft are unknown and are different from the undamaged aircraft plant dynamics, as can be seen from Eq. (38), the dynamic inversion controller $\hat{\boldsymbol{\delta}}$ will generate a dynamic inversion error $\boldsymbol{\varepsilon}$ as

$$\boldsymbol{\varepsilon} = \dot{\tilde{\boldsymbol{\omega}}} - \dot{\boldsymbol{\omega}}_d = \dot{\tilde{\boldsymbol{\omega}}} - \mathbf{F}_1\tilde{\boldsymbol{\omega}} - \mathbf{F}_2\boldsymbol{\sigma} - \mathbf{G}\hat{\boldsymbol{\delta}} \tag{46}$$

Comparing with Eq. (38), we see that the dynamic inversion error can also be expressed in terms of the unknown plant dynamics due to the damage effects

$$\boldsymbol{\varepsilon} = \Delta\dot{\boldsymbol{\omega}} = \Delta\mathbf{F}_1\tilde{\boldsymbol{\omega}} + \Delta\mathbf{F}_2\boldsymbol{\sigma} + \Delta\mathbf{G}\hat{\boldsymbol{\delta}} \tag{47}$$

For the dynamic inversion controller to track the reference-model angular acceleration vector $\dot{\boldsymbol{\omega}}_m$, the desired angular acceleration vector $\dot{\boldsymbol{\omega}}_d$ is set equal to

$$\dot{\boldsymbol{\omega}}_d = \dot{\boldsymbol{\omega}}_m + \mathbf{u}_e - \mathbf{u}_{\mathrm{ad}} \tag{48}$$

where $\mathbf{u}_{\mathrm{ad}}$ is an adaptive control augmentation signal designed to cancel out the dynamic inversion error, so that in an ideal setting, as the tracking error goes to zero asymptotically, the desired angular acceleration $\dot{\boldsymbol{\omega}}_d$ is equal to the reference-model angular acceleration $\dot{\boldsymbol{\omega}}_m$.

Substituting Eq. (48) into Eq. (46) results in

$$\boldsymbol{\varepsilon} = -\dot{\boldsymbol{\omega}}_e - \mathbf{u}_e + \mathbf{u}_{\mathrm{ad}} \tag{49}$$

We now obtain the following tracking error dynamics

$$\dot{\mathbf{e}} = \mathbf{A}\mathbf{e} + \mathbf{B}(\mathbf{u}_{\mathrm{ad}} - \boldsymbol{\varepsilon}) \tag{50}$$

where

$$\mathbf{e} = \left[\int_0^t \boldsymbol{\omega}_e\,\mathrm{d}\tau \quad \boldsymbol{\omega}_e\right]^T$$

and

$$\mathbf{A} = \begin{bmatrix} \mathbf{0} & \mathbf{I} \\ -\mathbf{K}_I & -\mathbf{K}_P \end{bmatrix}, \qquad \mathbf{B} = \begin{bmatrix} \mathbf{0} \\ \mathbf{I} \end{bmatrix}$$

The adaptive control augmentation vector $\mathbf{u}_{\mathrm{ad}}$ is based on the adaptation law by Rysdyk and Calise [10] with a modification to include additional product terms that appear in the nonlinear plant dynamics described by Eqs. (31–33):

$$\mathbf{u}_{\mathrm{ad}} = \mathbf{W}^T\boldsymbol{\beta}(\mathbf{C}_1, \mathbf{C}_2, \mathbf{C}_3, \mathbf{C}_4, \mathbf{C}_5, \mathbf{C}_6) \tag{51}$$

where $\boldsymbol{\beta}$ is a vector of basis functions computed using Kronecker products with $\mathbf{C}_i$, $i = 1, \ldots, 6$, as inputs into the neural network consisting of control commands, sensor feedback, and bias terms.

More specifically, the product terms are

$$\mathbf{C}_1 = V^2\begin{bmatrix} \boldsymbol{\omega}^T & \alpha\boldsymbol{\omega}^T & \beta\boldsymbol{\omega}^T \end{bmatrix} \tag{52}$$

$$\mathbf{C}_2 = V^2\begin{bmatrix} 1 & \alpha & \beta & \alpha^2 & \beta^2 & \alpha\beta & \alpha\beta^2 \end{bmatrix} \tag{53}$$

$$\mathbf{C}_3 = V^2\begin{bmatrix} \boldsymbol{\delta}^T & \alpha\boldsymbol{\delta}^T & \beta\boldsymbol{\delta}^T \end{bmatrix} \tag{54}$$

$$\mathbf{C}_4 = \begin{bmatrix} p\boldsymbol{\omega}^T & q\boldsymbol{\omega}^T & r\boldsymbol{\omega}^T \end{bmatrix} \tag{55}$$

$$\mathbf{C}_5 = \begin{bmatrix} u\boldsymbol{\omega}^T & v\boldsymbol{\omega}^T & w\boldsymbol{\omega}^T \end{bmatrix} \tag{56}$$

$$\mathbf{C}_6 = \begin{bmatrix} 1 & \theta & \phi & C_T \end{bmatrix} \tag{57}$$

The basis function is then expressed as

$$\boldsymbol{\beta} = \begin{bmatrix} \mathbf{C}_1 & \mathbf{C}_2 & \mathbf{C}_3 & \mathbf{C}_4 & \mathbf{C}_5 & \mathbf{C}_6 \end{bmatrix}^T \tag{58}$$

The network weights $\mathbf{W}$ are computed by a direct adaptive law, which incorporates a learning rate $\Gamma > 0$ and an e-modification term [22] $\mu > 0$ according to the following weight update law

$$\dot{\mathbf{W}} = -\Gamma(\boldsymbol{\beta}\mathbf{e}^T\mathbf{P}\mathbf{B} + \mu\|\mathbf{e}^T\mathbf{P}\mathbf{B}\|\mathbf{W}) \tag{59}$$

where the matrix $\mathbf{P}$ solves the Lyapunov equation $\mathbf{A}^T\mathbf{P} + \mathbf{P}^T\mathbf{A} = -\mathbf{Q}$ for some positive-definite matrix $\mathbf{Q}$ and $\|.\|$ is a Frobenius norm.

The e-modification term provides a robustness in the adaptive law [22]. The weight update law in Eq. (59) guarantees the stability of the neural network weights and the tracking error. The proof of this update law using the Lyapunov method is provided by Rysdyk and Calise [10]. Solving for the matrix $\mathbf{P}$ with $\mathbf{Q} = \mathbf{I}$, the weight update law can be rewritten as

$$\dot{\mathbf{W}} = -\Gamma(\boldsymbol{\beta}\mathbf{V} + \mu\|\mathbf{V}\|\mathbf{W}) \tag{60}$$

where

$$\mathbf{V} = \frac{1}{2}\boldsymbol{\omega}_e^T\mathbf{K}_p^{-1}\left(\mathbf{I} + \mathbf{K}_I^{-1}\right) + \frac{1}{2}\int_0^t \boldsymbol{\omega}_e^T\,\mathrm{d}\tau\mathbf{K}_I^{-1} \tag{61}$$

VI. Hybrid Direct–Indirect Adaptive Control Concept

Although the neural network direct adaptive law has been researched extensively and has been used with success in a number of applications, the possibility of a high-gain control due to aggressive learning can be a problem. Aggressive learning is characterized by setting the learning rate Γ high enough so as to reduce the dynamic inversion error rapidly. This can potentially lead to a control augmentation command that may saturate the control authority. A high-gain control may also excite unmodeled dynamics of the plant which can adversely affect the stability of the adaptive law. Control saturation and unmodeled dynamics have been addressed by Johnson et al. [19] and Hovakimyan et al. [14], but not in the context of a high-gain control associated with neural network direct adaptive control. Moreover, during a damage event, the knowledge of the plant dynamics of a damaged aircraft becomes impaired and, as a result, this can present a problem for a pilot to safely navigate the aircraft within a restricted flight envelope. For example, changes in stability and control derivatives can potentially cause a pilot to apply excessive or incorrect stick commands that could worsen the aircraft handling qualities. Direct adaptive control approaches accommodate changes in plant dynamics implicitly, but do not provide an explicit means for ascertaining the knowledge of the plant dynamics, which can potentially be used for developing damage detection and isolation strategies, as well as emergency flight planning, to provide guidance laws for energy management during a descent, approach, and landing. Toward this end, we introduce a modification to the present direct adaptive law to include an indirect adaptive law that provides an opportunity to perform an online estimation of the plant dynamics of the damaged aircraft explicitly. We call this approach a hybrid direct–indirect adaptive control. The indirect adaptive law will provide an estimate of the plant dynamics that will be used in the dynamic inversion. As a result, the control command will result in a smaller dynamic inversion error so that the learning of the direct adaptation neural network can be reduced. An architecture of the proposed hybrid adaptive control concept is shown in Fig. 7. In the current study, we have developed two indirect adaptive laws for the online estimation of the plant dynamics based on the Lyapunov stability theory and the recursive least-squares method.

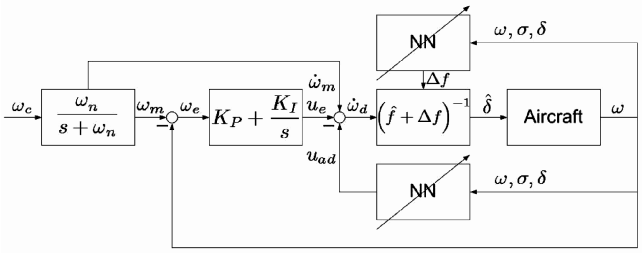

Fig. 7 Hybrid direct–indirect neural network adaptive flight control architecture.

A. Indirect Adaptive Control Method

In this approach, we would like to update the neural network weights using an indirect adaptive law that performs an online estimation of the incremental plant dynamics due to damage. Thus, if the damaged plant dynamics can be estimated, then the dynamic inversion controller can now be revised as

$$\hat{\boldsymbol{\delta}} = (\mathbf{G} + \Delta\hat{\mathbf{G}})^{-1}[\dot{\boldsymbol{\omega}}_d - (\mathbf{F}_1 + \Delta\hat{\mathbf{F}}_1)\tilde{\boldsymbol{\omega}} - (\mathbf{F}_2 + \Delta\hat{\mathbf{F}}_2)\boldsymbol{\sigma}] \tag{62}$$

where $\Delta\hat{\mathbf{F}}_1$, $\Delta\hat{\mathbf{F}}_2$, and $\Delta\hat{\mathbf{G}}$ are the estimated incremental plant matrices due to damage.

In an ideal situation, if the estimated damaged plant matrices are equal to the actual damaged plant matrices, then we would have a perfect tracking control. We now assume that the estimated damaged plant matrices can be expressed as

$$\Delta\hat{\mathbf{F}}_1 = \mathbf{W}_{\boldsymbol{\omega}}^T\boldsymbol{\beta}_{\boldsymbol{\omega}} \tag{63}$$

$$\Delta\hat{\mathbf{F}}_2 = \mathbf{W}_{\boldsymbol{\sigma}}^T\boldsymbol{\beta}_{\boldsymbol{\sigma}} \tag{64}$$

$$\Delta\hat{\mathbf{G}} = \mathbf{W}_{\boldsymbol{\delta}}^T\boldsymbol{\beta}_{\boldsymbol{\delta}} \tag{65}$$

where $\boldsymbol{\beta}_{\boldsymbol{\omega}}, \boldsymbol{\beta}_{\boldsymbol{\sigma}}$, and $\boldsymbol{\beta}_{\boldsymbol{\delta}}$ are some neural network basis functions, which are not necessarily the same as the basis function $\boldsymbol{\beta}$ for the direct adaptation neural network; and $\mathbf{W}_{\boldsymbol{\omega}}$, $\mathbf{W}_{\boldsymbol{\sigma}}$, and $\mathbf{W}_{\boldsymbol{\delta}}$ are the corresponding weight matrices.

The error dynamics can now be expressed as

$$\dot{\mathbf{e}} = \mathbf{A}\mathbf{e} + \mathbf{B}\mathbf{W}^T\boldsymbol{\beta} + \mathbf{B}\mathbf{W}_{\boldsymbol{\omega}}^T\boldsymbol{\beta}_{\boldsymbol{\omega}}\tilde{\boldsymbol{\omega}} + \mathbf{B}\mathbf{W}_{\boldsymbol{\sigma}}^T\boldsymbol{\beta}_{\boldsymbol{\sigma}}\boldsymbol{\sigma} + \mathbf{B}\mathbf{W}_{\boldsymbol{\delta}}^T\boldsymbol{\beta}_{\boldsymbol{\delta}}\hat{\boldsymbol{\delta}} - \mathbf{B}\boldsymbol{\varepsilon} \tag{66}$$

where $\boldsymbol{\varepsilon} = \Delta\dot{\boldsymbol{\omega}}$ is the dynamic inversion error.

We now propose the following indirect adaptive laws for the estimation of $\mathbf{W}_{\boldsymbol{\omega}}$, $\mathbf{W}_{\boldsymbol{\sigma}}$, and $\mathbf{W}_{\boldsymbol{\delta}}$:

$$\dot{\mathbf{W}}_{\boldsymbol{\omega}} = -\Gamma_{\boldsymbol{\omega}}\boldsymbol{\beta}_{\boldsymbol{\omega}}\tilde{\boldsymbol{\omega}}\mathbf{e}^T\mathbf{P}\mathbf{B} \tag{67}$$

$$\dot{\mathbf{W}}_{\boldsymbol{\sigma}} = -\Gamma_{\boldsymbol{\sigma}}\boldsymbol{\beta}_{\boldsymbol{\sigma}}\boldsymbol{\sigma}\mathbf{e}^T\mathbf{P}\mathbf{B} \tag{68}$$

$$\dot{\mathbf{W}}_{\boldsymbol{\delta}} = -\Gamma_{\boldsymbol{\delta}}\boldsymbol{\beta}_{\boldsymbol{\delta}}\hat{\boldsymbol{\delta}}\mathbf{e}^T\mathbf{P}\mathbf{B} \tag{69}$$

where $\Gamma_{\boldsymbol{\omega}}, \Gamma_{\boldsymbol{\sigma}}, \Gamma_{\boldsymbol{\delta}} > 0$ are the adaptation gains.

The proof is as follows:

We assume $\mathbf{A}$ is Hurwitz. We let $\mathbf{W} = \mathbf{W}^* + \tilde{\mathbf{W}}$, $\mathbf{W}_{\boldsymbol{\omega}} = \mathbf{W}_{\boldsymbol{\omega}}^* + \tilde{\mathbf{W}}_{\boldsymbol{\omega}}$, $\mathbf{W}_{\boldsymbol{\sigma}} = \mathbf{W}_{\boldsymbol{\sigma}}^* + \tilde{\mathbf{W}}_{\boldsymbol{\sigma}}$, and $\mathbf{W}_{\boldsymbol{\delta}} = \mathbf{W}_{\boldsymbol{\delta}}^* + \tilde{\mathbf{W}}_{\boldsymbol{\delta}}$, where the asterisk symbol denotes the ideal weight matrices that perfectly cancel out the dynamic inversion error $\boldsymbol{\varepsilon}$, and the tilde symbol denotes the weight deviations.

The ideal weight matrices are unknown but they may be assumed constant and bounded to stay within a $\boldsymbol{\Delta}$ neighborhood of the error $\boldsymbol{\varepsilon}$ defined as

$$\boldsymbol{\Delta} = \sup_{\tilde{\omega},\sigma,\hat{\delta}} |\mathbf{W}^{*T}\boldsymbol{\beta} + \mathbf{W}_{\omega}^{*T}\boldsymbol{\beta}_{\omega}\tilde{\omega} + \mathbf{W}_{\sigma}^{*T}\boldsymbol{\beta}_{\sigma}\boldsymbol{\sigma} + \mathbf{W}_{\delta}^{*T}\boldsymbol{\beta}_{\delta}\hat{\boldsymbol{\delta}} - \boldsymbol{\varepsilon}| \quad (70)$$

We now define the following Lyapunov candidate function

$$V = \mathbf{e}^T\mathbf{P}\mathbf{e} + \operatorname{tr}\left(\frac{\tilde{\mathbf{W}}^T\tilde{\mathbf{W}}}{\Gamma} + \frac{\tilde{\mathbf{W}}_{\omega}^T\tilde{\mathbf{W}}_{\omega}}{\Gamma_{\omega}} + \frac{\tilde{\mathbf{W}}_{\sigma}^T\tilde{\mathbf{W}}_{\sigma}}{\Gamma_{\sigma}} + \frac{\tilde{\mathbf{W}}_{\delta}^T\tilde{\mathbf{W}}_{\delta}}{\Gamma_{\delta}}\right) \quad (71)$$

where $\mathbf{P} \geq \mathbf{0}$ and tr(.) denotes the trace operator of a matrix.

The time derivative of the Lyapunov candidate function is then computed as

$$\dot{V} = \dot{\mathbf{e}}^T\mathbf{P}\mathbf{e} + \mathbf{e}^T\mathbf{P}\dot{\mathbf{e}} + 2\operatorname{tr}\left(\frac{\tilde{\mathbf{W}}^T\dot{\tilde{\mathbf{W}}}}{\Gamma} + \frac{\tilde{\mathbf{W}}_{\omega}^T\dot{\tilde{\mathbf{W}}}_{\omega}}{\Gamma_{\omega}} + \frac{\tilde{\mathbf{W}}_{\sigma}^T\dot{\tilde{\mathbf{W}}}_{\sigma}}{\Gamma_{\sigma}} + \frac{\tilde{\mathbf{W}}_{\delta}^T\dot{\tilde{\mathbf{W}}}_{\delta}}{\Gamma_{\delta}}\right) \quad (72)$$

Substituting Eqs. (59) and (66) into the preceding equation yields

$$\begin{aligned}\dot{V} = {} & -\mathbf{e}^T\mathbf{Q}\mathbf{e} + 2\mathbf{e}^T\mathbf{P}\mathbf{B}(\mathbf{W}^{*T} + \tilde{\mathbf{W}}^T)\boldsymbol{\beta} \\ & + 2\mathbf{e}^T\mathbf{P}\mathbf{B}\left(\mathbf{W}_{\omega}^{*T} + \tilde{\mathbf{W}}_{\omega}^T\right)\boldsymbol{\beta}_{\omega}\tilde{\omega} + 2\mathbf{e}^T\mathbf{P}\mathbf{B}\left(\mathbf{W}_{\sigma}^{*T} + \tilde{\mathbf{W}}_{\sigma}^T\right)\boldsymbol{\beta}_{\sigma}\boldsymbol{\sigma} \\ & + 2\mathbf{e}^T\mathbf{P}\mathbf{B}\left(\mathbf{W}_{\delta}^{*T} + \tilde{\mathbf{W}}_{\delta}^T\right)\boldsymbol{\beta}_{\delta}\hat{\boldsymbol{\delta}} - 2\mathbf{e}^T\mathbf{P}\mathbf{B}\boldsymbol{\varepsilon} \\ & + 2\operatorname{tr}\left[-\tilde{\mathbf{W}}^T\boldsymbol{\beta}\mathbf{e}^T\mathbf{P}\mathbf{B} - \mu\tilde{\mathbf{W}}^T\|\mathbf{e}^T\mathbf{P}\mathbf{B}\|(\mathbf{W}^* + \tilde{\mathbf{W}}) \right. \\ & \left. + \frac{\tilde{\mathbf{W}}_{\omega}^T\dot{\tilde{\mathbf{W}}}_{\omega}}{\Gamma_{\omega}} + \frac{\tilde{\mathbf{W}}_{\sigma}^T\dot{\tilde{\mathbf{W}}}_{\sigma}}{\Gamma_{\sigma}} + \frac{\tilde{\mathbf{W}}_{\delta}^T\dot{\tilde{\mathbf{W}}}_{\delta}}{\Gamma_{\delta}}\right] \end{aligned} \quad (73)$$

Using the trace property $\operatorname{tr}(\mathbf{AB}) = \operatorname{tr}(\mathbf{BA})$, we get

$$\mathbf{e}^T\mathbf{P}\mathbf{B}\tilde{\mathbf{W}}^T\boldsymbol{\beta} = \operatorname{tr}(\mathbf{e}^T\mathbf{P}\mathbf{B}\tilde{\mathbf{W}}^T\boldsymbol{\beta}) = \operatorname{tr}(\tilde{\mathbf{W}}^T\boldsymbol{\beta}\mathbf{e}^T\mathbf{P}\mathbf{B}) \quad (74)$$

$$\mathbf{e}^T\mathbf{P}\mathbf{B}\tilde{\mathbf{W}}_{\omega}^T\boldsymbol{\beta}_{\omega}\tilde{\omega} = \operatorname{tr}\left(\mathbf{e}^T\mathbf{P}\mathbf{B}\tilde{\mathbf{W}}_{\omega}^T\boldsymbol{\beta}_{\omega}\tilde{\omega}\right) = \operatorname{tr}\left(\tilde{\mathbf{W}}_{\omega}^T\boldsymbol{\beta}_{\omega}\tilde{\omega}\mathbf{e}^T\mathbf{P}\mathbf{B}\right) \quad (75)$$

$$\mathbf{e}^T\mathbf{P}\mathbf{B}\tilde{\mathbf{W}}_{\sigma}^T\boldsymbol{\beta}_{\sigma}\boldsymbol{\sigma} = \operatorname{tr}\left(\mathbf{e}^T\tilde{\mathbf{W}}_{\sigma}^T\boldsymbol{\beta}_{\sigma}\boldsymbol{\sigma}\right) = \operatorname{tr}\left(\tilde{\mathbf{W}}_{\sigma}^T\boldsymbol{\beta}_{\sigma}\boldsymbol{\sigma}\mathbf{e}^T\mathbf{P}\mathbf{B}\right) \quad (76)$$

$$\mathbf{e}^T\mathbf{P}\mathbf{B}\tilde{\mathbf{W}}_{\delta}^T\boldsymbol{\beta}_{\delta}\hat{\boldsymbol{\delta}} = \operatorname{tr}\left(\mathbf{e}^T\mathbf{P}\mathbf{B}\tilde{\mathbf{W}}_{\delta}^T\boldsymbol{\beta}_{\delta}\hat{\boldsymbol{\delta}}\right) = \operatorname{tr}\left(\tilde{\mathbf{W}}_{\delta}^T\boldsymbol{\beta}_{\delta}\hat{\boldsymbol{\delta}}\mathbf{e}^T\mathbf{P}\mathbf{B}\right) \quad (77)$$

Also, by completing the square, we have

$$\begin{aligned} & 2\operatorname{tr}[-\mu\tilde{\mathbf{W}}^T\|\mathbf{e}^T\mathbf{P}\mathbf{B}\|(\mathbf{W}^* + \tilde{\mathbf{W}})] \\ & \quad = -2\mu\|\mathbf{e}^T\mathbf{P}\mathbf{B}\|\left(\left\|\frac{\mathbf{W}^*}{2} + \tilde{\mathbf{W}}\right\|^2 - \left\|\frac{\mathbf{W}^*}{2}\right\|^2\right) \end{aligned} \quad (78)$$

Since $\dot{\tilde{\mathbf{W}}}_{\omega} = \dot{\mathbf{W}}_{\omega}$, $\dot{\tilde{\mathbf{W}}}_{\sigma} = \dot{\mathbf{W}}_{\sigma}$, and $\dot{\tilde{\mathbf{W}}}_{\delta} = \dot{\mathbf{W}}_{\delta}$, Eq. (73) then becomes

$$\begin{aligned}\dot{V} \leq {} & -\mathbf{e}^T\mathbf{Q}\mathbf{e} + 2\mathbf{e}^T\mathbf{P}\mathbf{B}\boldsymbol{\Delta} \\ & - 2\mu\|\mathbf{e}^T\mathbf{P}\mathbf{B}\|\left(\left\|\frac{\mathbf{W}*}{2} + \tilde{\mathbf{W}}\right\|^2 - \left\|\frac{\mathbf{W}*}{2}\right\|^2\right) \\ & + 2\operatorname{tr}\left[\tilde{\mathbf{W}}_{\omega}^T\left(\frac{\dot{\mathbf{W}}_{\omega}}{\Gamma_{\omega}} + \boldsymbol{\beta}_{\omega}\tilde{\omega}\mathbf{e}^T\mathbf{P}\mathbf{B}\right) + \tilde{\mathbf{W}}_{\sigma}^T\left(\frac{\dot{\mathbf{W}}_{\sigma}}{\Gamma_{\sigma}} + \boldsymbol{\beta}_{\sigma}\boldsymbol{\sigma}\mathbf{e}^T\mathbf{P}\mathbf{B}\right)\right. \\ & \left. + \tilde{\mathbf{W}}_{\delta}^T\left(\frac{\dot{\mathbf{W}}_{\delta}}{\Gamma_{\delta}} + \boldsymbol{\beta}_{\delta}\hat{\boldsymbol{\delta}}\mathbf{e}^T\mathbf{P}\mathbf{B}\right)\right] \end{aligned} \quad (79)$$

Since $\|\mathbf{B}\| = 1$, we establish that

$$\mathbf{e}^T\mathbf{Q}\mathbf{e} \leq \underline{\lambda}(\mathbf{Q})\|\mathbf{e}\|^2 \quad (80)$$

$$\mathbf{e}^T\mathbf{P}\mathbf{B}\boldsymbol{\Delta} \leq \rho(\mathbf{P})\|\mathbf{e}\|\|\boldsymbol{\Delta}\| \quad (81)$$

$$\|\mathbf{e}^T\mathbf{P}\mathbf{B}\|\left\|\frac{\mathbf{W}^*}{2}\right\|^2 \leq \rho(\mathbf{P})\|\mathbf{e}\|\left\|\frac{\mathbf{W}^*}{2}\right\|^2 \quad (82)$$

where $\underline{\lambda}(\mathbf{Q})$ is the minimum eigenvalue of $\mathbf{Q}$ and $\rho(\mathbf{P})$ is the spectral radius of $\mathbf{P}$.

To guarantee that $\dot{V} \leq 0$, we require that the trace operator be equal to zero, thus resulting in the indirect adaptive laws in Eqs. (67–69). In addition, we also require that

$$\|\mathbf{e}\| > \frac{\rho(\mathbf{P})}{2\underline{\lambda}(\mathbf{Q})}(4\|\boldsymbol{\Delta}\| + \mu\|\mathbf{W}^*\|^2) \quad (83)$$

The time rate of change of the Lyapunov candidate function is then strictly negative and, therefore, it would guarantee that the sinals are bounded. We note that $\dot{\mathbf{e}}, \tilde{\boldsymbol{\omega}}, \boldsymbol{\sigma}, \hat{\boldsymbol{\delta}} \in \mathcal{L}_{\infty}$, but $\mathbf{e} \in \mathcal{L}_2$ since

$$\underline{\lambda}(\mathbf{Q})\int_0^{\infty}\|\mathbf{e}\|^2\,\mathrm{d}t \leq V(0) \quad (84)$$

Using Eq. (83), we have

$$V(t \to \infty) \leq V(0) - 2\mu\underline{\lambda}(\mathbf{P})\int_0^{\infty}\|\mathbf{e}\|\left\|\frac{\mathbf{W}^*}{2} + \tilde{\mathbf{W}}\right\|^2\mathrm{d}t < \infty \quad (85)$$

Thus, the value of V as $t \to \infty$ and the tracking error $\mathbf{e}$ are uniformly bounded. Furthermore, if $\boldsymbol{\Delta} = \mathbf{0}$ and $\mu = 0$, we establish by means of the LaSalle–Yoshizawa theorem that

$$\lim_{t\to\infty}\|\mathbf{e}\| \to 0$$

so that $\|\dot{\mathbf{W}}\| \to 0$, $\|\dot{\mathbf{W}}_{\omega}\| \to 0$, $\|\dot{\mathbf{W}}_{\sigma}\| \to 0$, and $\|\dot{\mathbf{W}}_{\delta}\| \to 0$ as $t \to \infty$. This means that the indirect adaptive laws will result in a convergence of the estimated $\Delta\hat{\mathbf{F}}_1$, $\Delta\hat{\mathbf{F}}_2$, and $\Delta\hat{\mathbf{G}}$ to their steady-state values if there is no neural network approximation error. In addition, for the online estimation to converge to their correct values, the input signals must be sufficiently rich to excite all frequencies of interest in the plant dynamics. This condition is known as a persistent excitation (PE) and is defined as [20]

$$\boldsymbol{\alpha}_0 \leq \int_t^{t+T_0}\boldsymbol{\phi}(\tau)\boldsymbol{\phi}^T(\tau)\,\mathrm{d}\tau \leq \boldsymbol{\alpha}_1 \quad (86)$$

where $\boldsymbol{\phi} = [\,\tilde{\boldsymbol{\omega}}^T \quad \boldsymbol{\sigma}^T \quad \hat{\boldsymbol{\delta}}^T\,]^T$ and $\boldsymbol{\alpha}_0, \boldsymbol{\alpha}_1, T_0 > 0$.

We note that the indirect adaptive laws can be made more robust in a similar fashion as Eq. (60) to better handle unmodeled dynamics and disturbances with an addition of the e-modification term [22] to Eqs. (67–69) as

$$\dot{\mathbf{W}}_{\omega} = -\Gamma_{\omega}(\boldsymbol{\beta}_{\omega}\tilde{\omega}\mathbf{e}^T\mathbf{P}\mathbf{B} + \mu_{\omega}\|\mathbf{e}^T\mathbf{P}\mathbf{B}\|\mathbf{W}_{\omega}) \quad (87)$$

$$\dot{\mathbf{W}}_{\sigma} = -\Gamma_{\sigma}(\boldsymbol{\beta}_{\sigma}\boldsymbol{\sigma}\mathbf{e}^T\mathbf{P}\mathbf{B} + \mu_{\sigma}\|\mathbf{e}^T\mathbf{P}\mathbf{B}\|\mathbf{W}_{\sigma}) \quad (88)$$

$$\dot{\mathbf{W}}_{\delta} = -\Gamma_{\delta}(\boldsymbol{\beta}_{\delta}\hat{\boldsymbol{\delta}}\mathbf{e}^T\mathbf{P}\mathbf{B} + \mu_{\delta}\|\mathbf{e}^T\mathbf{P}\mathbf{B}\|\mathbf{W}_{\delta}) \quad (89)$$

in which case the time rate of change of the Lyapunov candidate function becomes

$$\dot{V} \le -2\mu\|\mathbf{e}^T\mathbf{PB}\|\left\|\frac{\mathbf{W}^*}{2}+\tilde{\mathbf{W}}\right\|^2 - 2\mu_\omega\|\mathbf{e}^T\mathbf{PB}\|\left\|\frac{\tilde{\mathbf{W}}_\omega^*}{2}+\tilde{\mathbf{W}}_\omega\right\|^2 - 2\mu_\sigma\|\mathbf{e}^T\mathbf{PB}\| \times \left\|\frac{\tilde{\mathbf{W}}_\sigma^*}{2}+\tilde{\mathbf{W}}_\sigma\right\|^2 - 2\mu_\delta\|\mathbf{e}^T\mathbf{PB}\|\left\|\frac{\tilde{\mathbf{W}}_\delta^*}{2}+\tilde{\mathbf{W}}_\delta\right\|^2 \tag{90}$$

The effect of the e-modification, therefore, is to increase the negative time rate of change of the Lyapunov candidate function so that, as long as the effects of unmodeled dynamics and/or disturbances do not exceed the value of $\dot{V}$, the adaptive signals should remain bounded. The e-modification thus makes the adaptive law more robust to unmodeled dynamics [23].

It should be noted that we have so far assumed that $\tilde{\boldsymbol{\omega}}, \boldsymbol{\sigma}, \hat{\boldsymbol{\delta}} \in \mathcal{L}_\infty$. Suppose that the input signals become unbounded, i.e., $\tilde{\boldsymbol{\omega}}$, $\boldsymbol{\sigma}$, $\hat{\boldsymbol{\delta}} \notin \mathcal{L}_\infty$; the adaptive laws in Eqs. (67–69) will become unstable because of the signal unboundedness. In this situation, we need to modify the adaptive laws to handle unbounded signals by a normalization method [20]. By normalization, we mean to consider alternate input signals that are bounded even though the original input signals are unbounded. Toward that end, we note that $\tilde{\boldsymbol{\omega}}(1+\tilde{\boldsymbol{\omega}}^T\mathbf{R}_\omega\tilde{\boldsymbol{\omega}})^{-1} \in \mathcal{L}_\infty$ even though $\tilde{\boldsymbol{\omega}} \notin \mathcal{L}_\infty$ since

$$\lim_{\tilde{\omega}\to\infty}\frac{\tilde{\boldsymbol{\omega}}}{1+\tilde{\boldsymbol{\omega}}^T\mathbf{R}_\omega\tilde{\boldsymbol{\omega}}} = \mathbf{0} \tag{91}$$

where $\mathbf{R}_\omega$ is a positive-definite weight matrix.

Similar considerations can be made for $\boldsymbol{\sigma}$ and $\hat{\boldsymbol{\delta}}$. Using these alternate input signals, we obtain the following normalized indirect adaptive laws for unbounded signals:

$$\dot{\mathbf{W}}_\omega = -\Gamma_\omega(1+\tilde{\boldsymbol{\omega}}^T\mathbf{R}_\omega\tilde{\boldsymbol{\omega}})^{-1}(\boldsymbol{\beta}_\omega\tilde{\boldsymbol{\omega}}\mathbf{e}^T\mathbf{PB} + \mu_\omega\|\mathbf{e}^T\mathbf{PB}\|\mathbf{W}_\omega) \tag{92}$$

$$\dot{\mathbf{W}}_\sigma = -\Gamma_\sigma(1+\boldsymbol{\sigma}^T\mathbf{R}_\sigma\boldsymbol{\sigma})^{-1}(\boldsymbol{\beta}_\sigma\boldsymbol{\sigma}\mathbf{e}^T\mathbf{PB} + \mu_\sigma\|\mathbf{e}^T\mathbf{PB}\|\mathbf{W}_\sigma) \tag{93}$$

$$\dot{\mathbf{W}}_\delta = -\Gamma_\delta(1+\hat{\boldsymbol{\delta}}^T\mathbf{R}_\delta\hat{\boldsymbol{\delta}})^{-1}(\boldsymbol{\beta}_\delta\hat{\boldsymbol{\delta}}\mathbf{e}^T\mathbf{PB} + \mu_\delta\|\mathbf{e}^T\mathbf{PB}\|\mathbf{W}_\delta) \tag{94}$$

B. Recursive Least-Squares Method

An alternate approach that may be considered in lieu of the indirect adaptive law discussed in the previous section is a recursive least-squares (RLS) method for identifying the damaged plant dynamics, based on the dynamic inversion or modeling error, instead of the tracking error as in the indirect adaptive law. Suppose the dynamic inversion error can be written as

$$\boldsymbol{\varepsilon} = \boldsymbol{\Phi}^T\boldsymbol{\theta} + \Delta\boldsymbol{\varepsilon} \tag{95}$$

where $\boldsymbol{\Phi}^T = [\mathbf{W}_\omega^T \;\; \mathbf{W}_\sigma^T \;\; \mathbf{W}_\delta^T]$, $\boldsymbol{\theta} = [\tilde{\boldsymbol{\omega}}^T \;\; \boldsymbol{\beta}_\omega^T \;\; \boldsymbol{\sigma}^T \;\; \boldsymbol{\beta}_\sigma^T \;\; \hat{\boldsymbol{\delta}}^T \;\; \boldsymbol{\beta}_\delta^T]^T$, and $\Delta\boldsymbol{\varepsilon}$ is the computational error in the estimated dynamic inversion error $\hat{\boldsymbol{\varepsilon}}$ defined as

$$\hat{\boldsymbol{\varepsilon}} = \dot{\hat{\boldsymbol{\omega}}} - \mathbf{F}_1\tilde{\boldsymbol{\omega}} - \mathbf{F}_2\boldsymbol{\sigma} - \mathbf{G}\hat{\boldsymbol{\delta}} \tag{96}$$

where $\dot{\hat{\boldsymbol{\omega}}}$ is the estimated angular acceleration which may be subject to computational errors.

Generally, the angular acceleration may not be available from rate gyro sensors. In such a case, one method of estimating $\dot{\hat{\boldsymbol{\omega}}}$ is to use a backward finite difference method

$$\dot{\hat{\boldsymbol{\omega}}}_j = \frac{\tilde{\boldsymbol{\omega}}_j - \tilde{\boldsymbol{\omega}}_{j-1}}{\Delta t} \tag{97}$$

to estimate $\dot{\hat{\boldsymbol{\omega}}}$ at the jth time step, but this method can result in a significant error if Δt is either too small or too large.

Another approach is to sample aircraft rate data and use them to generate an, at least, C^1 smooth curve in time using a cubic or B-spline method. This curve is then differentiated at the spline knots to find the estimated derivative values. In either case, the derivative computation will introduce an error source $\Delta\boldsymbol{\varepsilon}$. If the error is unbiased, i.e., it can be characterized as a white noise about the mean value, then the recursive least-squares method can be applied to estimate the damaged plant dynamics. The white noise can be minimized using an optimal estimation method by considering the following cost function

$$J(\boldsymbol{\Phi}) = \frac{1}{2}\int_0^t (1+\xi)^{-1}\|\hat{\boldsymbol{\varepsilon}} - \boldsymbol{\Phi}^T\boldsymbol{\theta}\|\,\mathrm{d}\tau \tag{98}$$

where the factor $1+\xi$ is a normalization factor defined as

$$1+\xi = 1+\boldsymbol{\theta}^T\mathbf{R}\boldsymbol{\theta} \tag{99}$$

and $\mathbf{R}$ is a positive-definite weight matrix.

To minimize the cost function, we compute its gradient with respect to the weight matrix and set it to zero, thus resulting in

$$\frac{\partial J^T}{\partial\boldsymbol{\Phi}} = -\int_0^t (1+\xi)^{-1}\boldsymbol{\theta}(\hat{\boldsymbol{\varepsilon}}^T - \boldsymbol{\theta}^T\boldsymbol{\Phi})\,\mathrm{d}\tau = \mathbf{0} \tag{100}$$

Equation (100) is then written as

$$\int_0^t (1+\xi)^{-1}\boldsymbol{\theta}\boldsymbol{\theta}^T\,\mathrm{d}\tau\boldsymbol{\Phi} = \int_0^t (1+\xi)^{-1}\boldsymbol{\theta}\hat{\boldsymbol{\varepsilon}}^T\,\mathrm{d}\tau \tag{101}$$

Let

$$\mathbf{R}^{-1} = \int_0^t (1+\xi)^{-1}\boldsymbol{\theta}\boldsymbol{\theta}^T\,\mathrm{d}\tau > \mathbf{0} \tag{102}$$

We note that

$$\mathbf{R}^{-1}\mathbf{R} = \mathbf{I} \Rightarrow \dot{\mathbf{R}}^{-1}\mathbf{R} + \mathbf{R}^{-1}\dot{\mathbf{R}} = \mathbf{0} \tag{103}$$

Differentiating Eq. (101) yields

$$\mathbf{R}^{-1}\dot{\boldsymbol{\Phi}} + (1+\xi)^{-1}\boldsymbol{\theta}^T\boldsymbol{\Phi} = (1+\xi)^{-1}\boldsymbol{\theta}\hat{\boldsymbol{\varepsilon}}^T \tag{104}$$

From Eqs. (103) and (104), we obtain the following recursive least-squares weight update laws

$$\dot{\boldsymbol{\Phi}} = (1+\xi)^{-1}\mathbf{R}\boldsymbol{\theta}(\hat{\boldsymbol{\varepsilon}}^T - \boldsymbol{\theta}^T\boldsymbol{\Phi}) \tag{105}$$

$$\dot{\mathbf{R}} = -(1+\xi)^{-1}\mathbf{R}\boldsymbol{\theta}\boldsymbol{\theta}^T\mathbf{R} \tag{106}$$

The matrix $\mathbf{R}$ is called the covariance matrix and the recursive least-squares formula has a very similar form to the Kalman filter with Eq. (106) as the differential Riccati equation for zero-order plant dynamics.

The recursive least-squares weight update law can be shown to be stable and result in bounded signals. To show this, we let $\boldsymbol{\Phi} = \boldsymbol{\Phi}^* + \tilde{\boldsymbol{\Phi}}$, with the asterisk and tilde symbols denoting ideal weights and weight deviations, respectively. We choose the following Lyapunov candidate function

$$L = V + \mathrm{tr}(\tilde{\boldsymbol{\Phi}}^T\mathbf{R}^{-1}\tilde{\boldsymbol{\Phi}}) \tag{107}$$

where V is the Lyapunov candidate function for the direct neural network adaptive control, and we have established that $\dot{V} \le 0$.

The time rate of change of the Lyapunov candidate function is computed as

$$\dot{L} = \dot{V} + \mathrm{tr}(2\tilde{\boldsymbol{\Phi}}^T\mathbf{R}^{-1}\dot{\tilde{\boldsymbol{\Phi}}} + \tilde{\boldsymbol{\Phi}}^T\dot{\mathbf{R}}^{-1}\tilde{\boldsymbol{\Phi}}) \tag{108}$$

The weight matrix $\mathbf{\Phi}$ can be shown to converge to the ideal weights $\mathbf{\Phi}^*$ [20] so that

$$\dot{\tilde{\mathbf{\Phi}}} = -(1+\xi)^{-1}\mathbf{R}\boldsymbol{\theta}\boldsymbol{\theta}^T\tilde{\mathbf{\Phi}} \tag{109}$$

Substituting Eq. (109) into Eq. (108) results in

$$\dot{L} = \dot{V} - (1+\xi)^{-1}\mathrm{tr}(\tilde{\mathbf{\Phi}}^T\boldsymbol{\theta}\boldsymbol{\theta}^T\tilde{\mathbf{\Phi}}) \le 0 \tag{110}$$

Thus, the recursive least-squares weight update law is stable.

The recursive least-squares method can be implemented in either continuous time or discrete time. A continuous-time estimation requires solving the differential Eqs. (105) and (106) at every time step. On the other hand, the discrete-time sampling estimation provides more flexibility, in that the estimation can be executed after a specified number of data points have been collected. This would improve the PE condition of the input signals. In the actual implementation of the hybrid adaptive flight control algorithm, we use the following discrete-time recursive least-squares weight update law with an adaptive or directional forgetting factor [24]

$$\mathbf{\Phi}_{i+1} = \mathbf{\Phi}_i + (1+\xi_{i+1})^{-1}\mathbf{R}_{i+1}\boldsymbol{\theta}_i\left(\hat{\boldsymbol{\varepsilon}}_{i+1}^T - \boldsymbol{\theta}_i^T\mathbf{\Phi}_i\right) \tag{111}$$

$$\mathbf{R}_{i+1} = \mathbf{R}_i - \left(\psi_{i+1}^{-1} + \xi_{i+1}\right)^{-1}\mathbf{R}_i\boldsymbol{\theta}_i\boldsymbol{\theta}_i^T\mathbf{R}_i \tag{112}$$

where ψ is defined as

$$\psi_{i+1} = \varphi_{i+1} - \xi_i^{-1}(1-\varphi_{i+1}) \tag{113}$$

The parameter $\boldsymbol{\varphi}$ is called a directional forgetting factor which can be computed using the following adaptive law at each sampling period

$$\boldsymbol{\varphi}_{i+1}^{-1} = 1 + (1+\rho)\,\ell_n(1+\xi_{i+1}) + \left[\frac{\eta_{i+1}(1+\vartheta_{i+1})}{1+\xi_{i+1}+\eta_{i+1}} - 1\right]\frac{\xi_{i+1}}{1+\xi_{i+1}} \tag{114}$$

where ρ is a constant, and η and ϑ are parameters with the following update laws

$$\eta_{i+1} = \lambda_{i+1}^{-1}\|\hat{\boldsymbol{\varepsilon}}_{i+1} - \mathbf{\Phi}_i^T\boldsymbol{\theta}_i\|^2 \tag{115}$$

$$\vartheta_{i+1} = \varphi_{i+1}(1+\vartheta_i) \tag{116}$$

$$\lambda_{k+1} = \varphi_{i+1}[\lambda_k + (1+\xi_{i+1})\|\hat{\boldsymbol{\varepsilon}}_{i+1} - \mathbf{\Phi}_i^T\boldsymbol{\theta}_i\|^2] \tag{117}$$

VII. Control Simulations

To evaluate the hybrid adaptive flight control with the indirect adaptive law and the recursive least-squares method, a simulation was performed in the MATLAB environment. A damage configuration corresponding to a 30% loss of the left wing for the GTM is selected. The direct adaptation neural network is a single-layer sigma-pi network. Pilot commands are simulated by a series of step input pitch doublets. The tracking performance of the three adaptive control schemes is compared in Fig. 8.

It can be seen that the hybrid indirect adaptive control scheme offers some degree of improvement in the tracking performance as compared with the direct adaptive control scheme. In contrast, the hybrid recursive least-squares adaptive control scheme is seen to perform better than both the direct and hybrid indirect adaptive control schemes, as it provides the best tracking performance of the pitch channel command. It is noted that both the direct and hybrid indirect adaptive control schemes are improving with time as the tracking errors decrease asymptotically.

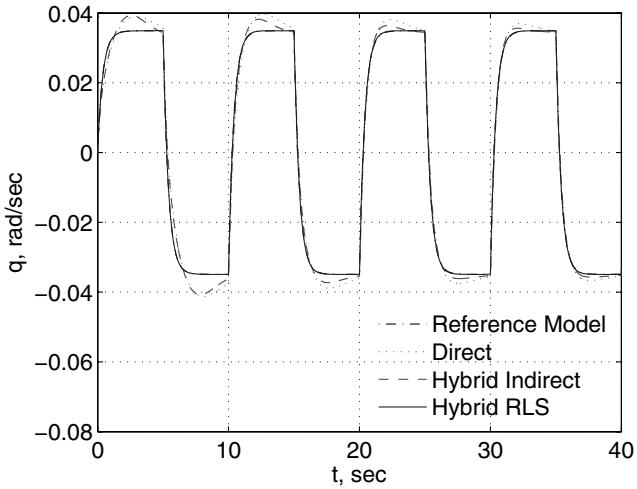

Fig. 8 Pitch doublet tracking performance.

Figures 9 and 10 are the roll and yaw rate responses during the pitch doublet maneuver. Because of the asymmetric wing damage, the roll performance of the aircraft should be expected to be most affected. The hybrid recursive least-squares adaptive control scheme is able to regulate the roll and yaw rates much better than both the direct and hybrid adaptive control schemes. In fact, the roll response

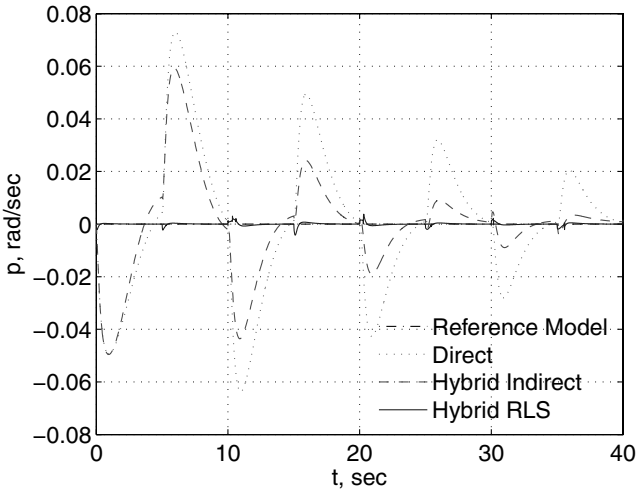

Fig. 9 Roll response.

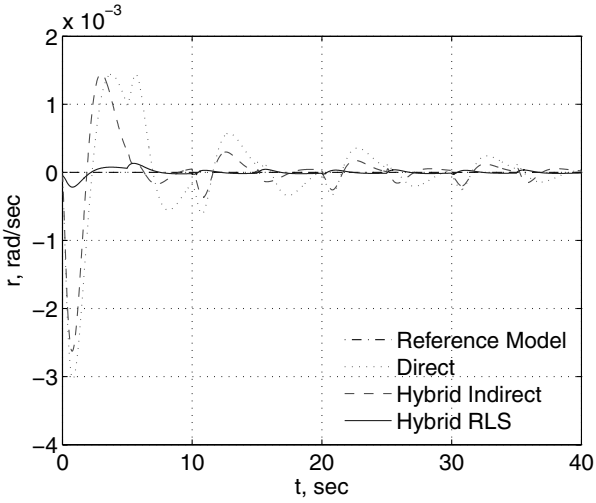

Fig. 10 Yaw response.

for the direct adaptive control scheme is not considered acceptable because the roll rate amplitude is quite significant as compared with the pitch rate amplitude. To a lesser extent, the poor roll performance also is seen with the hybrid indirect adaptive control scheme during the first two pitch doublets.

Figure 11 shows the norms of the roll, pitch, and yaw rate tracking errors for the three adaptive control schemes. As can be seen, the hybrid recursive least-squares adaptive control scheme achieves the smallest tracking error norm, whereas the hybrid indirect adaptive control scheme shows a reasonably good improvement in the tracking error norm over the direct adaptive control scheme. After only two pitch doublets, the tracking error norm for the hybrid indirect adaptive control scheme reduces to more than half of the tracking error norm for the direct adaptive control scheme.

The aileron, elevator, and rudder commands to achieve the pitch doublet maneuver are as shown in Figs. 12–14, respectively. Because of the cross coupling between the longitudinal and lateral motions as a result of the wing damage, the pitch maneuver requires all of the three control surface command inputs. Figure 12 shows the remaining right aileron command input needed to compensate for the rolling moment during the pitch doublet maneuver due to the pitch-roll coupling effect of wing damage. The aileron command input computed by the hybrid recursive least-squares adaptive control scheme is well formed, whereas the aileron commands from both the direct and hybrid indirect adaptive control schemes exhibit some initial overshoots and lags; however, after three pitch doublets, the aileron command for the hybrid indirect adaptive scheme converges to that of the recursive least-squares adaptive control scheme.

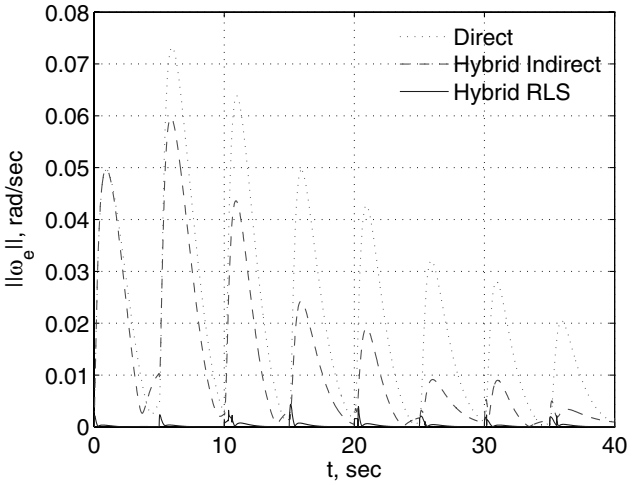

Fig. 11 Tracking error norm.

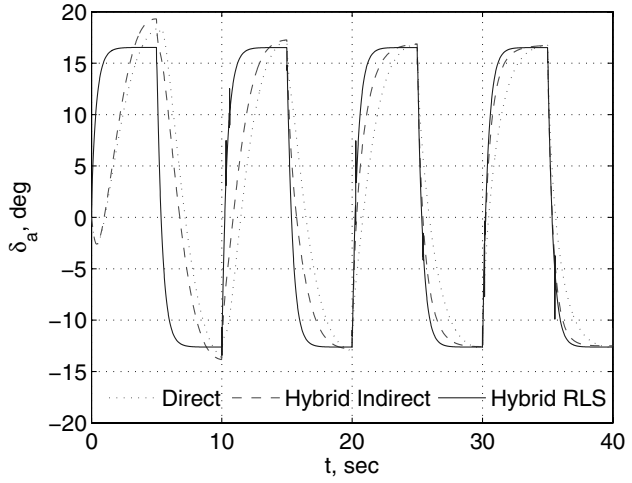

Fig. 12 Aileron command.

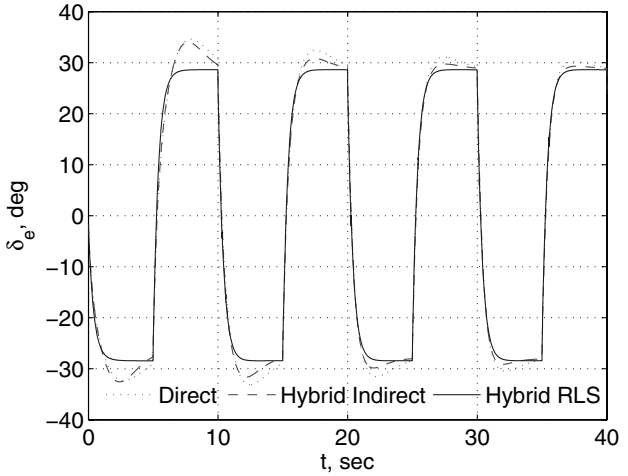

Fig. 13 Elevator command.

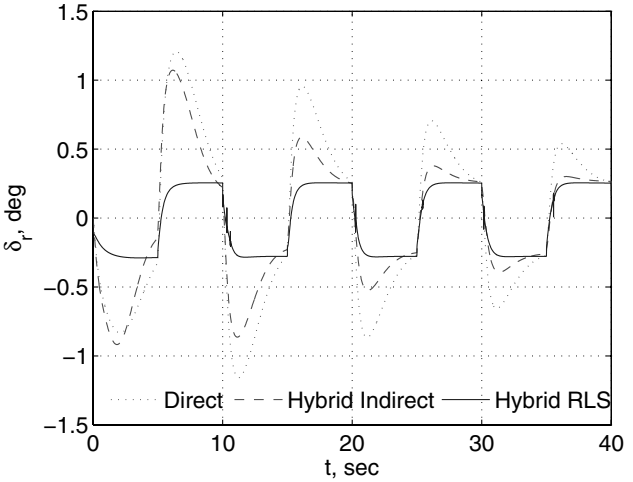

Fig. 14 Rudder command.

Figure 13 is the elevator command inputs computed by the three adaptive control schemes to achieve the pitch channel command. The elevator commands computed by the direct and hybrid indirect adaptive control schemes exhibit some initial overshoots, but the hybrid indirect adaptive control scheme reduces the overshoot amplitude to some extent. The hybrid recursive least-squares adaptive control scheme results in a very well-formed elevator command input without any noticeable overshoot.

Figure 14 is the rudder command input needed to compensate for the adverse yawing moment during the pitch doublet maneuver. Both the direct and hybrid indirect adaptive control schemes produce rudder command inputs that are quite aggressive, but after only one pitch doublet, the hybrid indirect adaptive control scheme begins to improve as the overshoot amplitude begins to attenuate. Again, the hybrid recursive least-squares adaptive control scheme produces a very well-formed rudder command input.

For this simulation, actuator dynamics are not included. In a situation where an adaptive control scheme generates a high-gain control signal, a control surface command input can encounter an actuator rate limiting, which can potentially result in pilot-induced oscillations (PIO) [25]. Therefore, the effect of a high-gain control in adaptive control should be avoided.

VIII. Discussions

In the current adaptive flight control study, only traditional control effectors that include ailerons, elevators, and rudder are used. In severe damage situations, these control effectors may not be sufficient to stabilize and maintain good handling qualities of a

damaged aircraft. Therefore, any adaptive flight control method must include a control allocation strategy that uses other potential control effectors that are otherwise not used in a conventional flight control system. These control effectors can include engine thrust for pitch control, engine differential thrust for yaw control, wing spoilers for roll control, and others. The problems of time-scale separation due to actuator dynamics are important for systems with a different time latency such as engines. Traditionally, systems with slow–fast dynamics can be appropriately handled by the singular perturbation method [26]. For flight control applications, engine dynamics are usually not known and typically possess a variable time delay, which can pose a challenge to a flight control system augmented with propulsion as a means for controlling an aircraft. Adaptive control strategies incorporating propulsion have been investigated, but some of these studies do not include slow dynamic models of aircraft engines [13].

Damage effects can present a serious challenge to a flight control system, because a damaged aircraft would no longer behave nominally because its stability and control characteristics could be changed significantly. Although neural network adaptive control offers a promise for an online learning capability to enable a flight control system to adapt to changes in flight dynamics of a damaged aircraft, the current reality is that adaptive control is still far from being accepted for use as a primary flight control system, due to challenging problems with verification and validation of adaptive systems. Although the proposed hybrid adaptive control approach appears promising in resolving the concern with a high-gain control, the problems with the convergence and global stability of neural networks are still being researched.

Integrated flight dynamic modeling is another area of research that needs to be addressed. Integrated flight dynamic modeling develops a better understanding of benefits and limitations of adaptive flight control methods through simulations and validation. An integrated flight dynamic model would be able to predict the combined effects of aerodynamics, rigid body aircraft dynamics, structural dynamics of the airframe, and engine dynamics, as well flight control actuator dynamics. The integrated model can provide a way to quantitatively assess the effect of unmodeled dynamics on the robustness of adaptive control methods.

Structural interactions with a flight control system are critical to any flight control development [27–29]. Elastic deflections and mode shapes can adversely contribute to the vehicle stability and control, resulting in problems such as flutter, control reversal, and structural frequency interactions inside a flight control bandwidth. Adaptive flight control methods will need to observe and obey structural load constraints imposed by a damaged airframe. This would mean that feedback signals generated by a flight control system must maintain adequate structural margins. However, this can be challenging because structural margins may become uncertain when a damage occurs. Another issue is associated with elastic modes shifting due to changes in the structural stiffness and mass of the airframe. Structural frequency shifts can reduce the effectiveness of aeroservoelastic notch filters present in a typical flight control system. Adaptive output feedback control can potentially offer a strategy for addressing structural interactions with a flight control system [30].

IX. Conclusions

This paper has presented some recent results on the modeling, control, and simulation study for a damaged generic transport model. Aerodynamic modeling has been performed to provide an understanding of the damage effects on the control and stability characteristics. The modeling results reveal aerodynamic and control coupling in all of the three stability axes. A flight dynamic model has been developed to account for changes in aerodynamics and mass properties of a damaged aircraft. A neural network hybrid adaptive flight control concept has been developed to enable damaged plant dynamics to be estimated via an indirect adaptive law or a recursive least-squares method that works in conjunction with a direct adaptive control strategy. Control simulations have been performed for a wing damage to evaluate the effectiveness of the hybrid adaptive control. The results show that the hybrid adaptive control can provide significant improvement in the tracking performance over the direct adaptive control, particularly with the hybrid recursive least-squares method. The hybrid adaptive control method offers some advantages in reducing the possibility of a high-gain control and providing improved knowledge of the damaged plant dynamics, which can potentially be used for developing damage detection and isolation strategies as well as emergency flight planning methods. Future work will investigate the robustness of the proposed hybrid adaptive control method in the presence of sensor noise and exogenous disturbances. Moreover, future work will also investigate integrated adaptive flight control with propulsion and airframe effects to address aeroservoelastic effects and slow engine dynamics.

References

[1] National Transportation Safety Board, "In-Flight Separation of Vertical Stabilizer American Airlines Flight 587 Airbus Industrie A300-605R, N14053 Belle Harbor, New York, November 12, 2001," NTSB/AAR-04/04, 2004.

[2] Lemaignan, B., "Flying with No Flight Controls: Handling Qualities Analyses of the Baghdad Event," *AIAA Atmospheric Flight Mechanics Conference*, AIAA 2005-5907, 2005.

[3] National Transportation Safety Board, "United Airlines Flight 232 McDonnell-Douglas DC-10-10, Sioux Gateway Airport, Sioux City, Iowa, July 19, 1989," NTSB/AAR90-06, 1990.

[4] Burcham, F. W., Jr., and Fullerton, C. G., "Controlling Crippled Aircraft: With Throttles," NASA TM-104238, 1991.

[5] Belcastro, C. M., "Integrated Resilient Aircraft Control Project Proposal," NASA Aeronautics Research Mission Directorate Internal Document, 2006.

[6] Kaneshige, J., Bull, J., and Totah, J., "Generic Neural Flight Control and Autopilot System," *AIAA Guidance, Navigation, and Control Conference*, AIAA 2000-4281, 2000.

[7] Atkins, E., "Dynamic Waypoint Generation Given Reduced Flight Performance," *42nd AIAA Aerospace Sciences Meeting and Exhibit*, AIAA 2004-779, 2004.

[8] Jacklin, S. A., Schumann, J. M., Gupta, P. P., Richard, R., Guenther, K., and Soares, F., "Development of Advanced Verification and Validation Procedures and Tools for the Certification of Learning Systems in Aerospace Applications," *AIAA Infotech@Aerospace Conference*, AIAA 2005-69122005.

[9] Steinberg, M. L., "Comparison of Intelligent, Adaptive, and Nonlinear Flight Control Laws," *AIAA Guidance, Navigation, and Control Conference*, AIAA 1999-4044, 1999.

[10] Rysdyk, R. T., and Calise, A. J., "Fault Tolerant Flight Control via Adaptive Neural Network Augmentation," *AIAA Guidance, Navigation, and Control Conference*, AIAA 1998-4483, 1998.

[11] Kim, B. S., and Calise, A. J., "Nonlinear Flight Control Using Neural Networks," *Journal of Guidance, Control, and Dynamics*, Vol. 20, No. 1, 1997, pp. 26–33.

[12] Idan, M., Johnson, M. D., and Calise, A. J., "Hierarchical Approach to Adaptive Control for Improved Flight Safety," *Journal of Guidance, Control and Dynamics*, Vol. 25, No. 6, 2002, pp. 1012–1020.

[13] Idan, M., Johnson, M. D., Calise, A. J., and Kaneshige, J., "Intelligent Aerodynamic/Propulsion Flight Control For Flight Safety: A Nonlinear Adaptive Approach," *Proceedings of the American Control Conference*, Inst. of Electrical and Electronics Engineers, New York, June 2001, pp. 2918–2923.

[14] Hovakimyan, N., Kim, N., Calise, A. J., Prasad, J. V. R., and Corban, E. J., "Adaptive Output Feedback for High-Bandwidth Control of an Unmanned Helicopter," *AIAA Guidance, Navigation and Control Conference*, AIAA 2001-4181, 2001.

[15] Bailey, R. M., Hostetler, R. W., Barnes, K. N., Belcastro, C. M., and Belcastro, C. M., "Experimental Validation: Subscale Aircraft Ground Facilities and Integrated Test Capability," *AIAA Guidance, Navigation, and Control Conference*, AIAA 2005-6433, 2005.

[16] Totah, J., Kinney, D., Kaneshige, J., and Agabon, S., "Integrated Vehicle Modeling Environment," *AIAA Atmospheric Flight Mechanics Conference and Exhibit*, AIAA 1999-4106, 1999.

[17] Rohrs, C. E., Valavani, L., Athans, M., and Stein, G., "Robustness of Continuous-Time Adaptive Control Algorithms in the Presence of Unmodeled Dynamics," *IEEE Transactions on Automatic Control*, Vol 30, No. 9, 1985, pp. 881–889. doi:10.1109/TAC.1985.1104070

[18] Eberhart, R. L., and Ward, D. G., "Indirect Adaptive Flight Control

System Interactions," *International Journal of Robust and Nonlinear Control*, Vol. 9, No. 14, 1999, pp. 1013–1031. doi:10.1002/(SICI)1099-1239(19991215)9:14<1013::AID-RNC450>3.0.CO;2-4

[19] Johnson, E. N., Calise, A. J., El-Shirbiny, H. A., and Rysdyk, R. T., "Feedback Linearization with Neural Network Augmentation Applied to X-33 Attitude Control," *AIAA Guidance, Navigation, and Control Conference*, AIAA 2000-4157, 2000.

[20] Ioannu, P. A., and Sun, J., *Robust Adaptive Control*, Prentice–Hall, Englewood Cliffs, NJ, 1996.

[21] Krishnakumar, K., Limes, G., Gundy-Burlet, K., and Bryant, D., "Adaptive Critic Approach to Reference Model Adaptation," *AIAA Guidance, Navigation, and Control Conference*, AIAA 2003-5790, 2003.

[22] Narendra, K. S., and Annaswamy, A. M., "New Adaptive Law for Robust Adaptation Without Persistent Excitation," *IEEE Transactions on Automatic Control*, Vol. 32, No. 2, 1987, pp. 134–145. doi:10.1109/TAC.1987.1104543

[23] Lewis, F. W., Jagannathan, S., and Yesildirak, A., *Neural Network Control of Robot Manipulators and Non-Linear Systems*, CRC Press, Boca Raton, FL, 1998.

[24] Bobal, V., *Digital Self-Tuning Controllers: Algorithms, Implementation, and Applications*, Springer–Verlag, London, 2005.

[25] Gilbreath, G. P., "Prediction of Pilot-Induced Oscillations (PIO) due to Actuator Rate Limiting Using the Open-Loop Onset Point (OLOP) Criterion," M.S. Thesis, Air Force Inst. of Technology, Wright-Patterson AFB, OH, 2001.

[26] Naidu, D. S., and Calise, A. J., "Singular Perturbations and Time Scales in Guidance and Control of Aerospace Systems: A Survey," *Journal of Guidance, Control, and Dynamics*, Vol. 24, No. 6, 2001, pp. 1057–1078.

[27] Brenner, M. J., and Prazenica, R. J., "Aeroservoelastic Model Validation and Test Data Analysis of the F/A-18 Active Aeroelastic Wing," NASA TM-2003-212021, 2003.

[28] Meirovitch, L., and Tuzcu, I., "Integrated Approach to Flight Dynamics and Aeroservoelasticity of Whole Flexible Aircraft, Part 1: System Modeling," *AIAA Guidance, Navigation, and Control Conference*, AIAA 2002-4747, 2002.

[29] Meirovitch, L., and Tuzcu, I., "Integrated Approach to Flight Dynamics and Aeroservoelasticity of Whole Flexible Aircraft, Part 2: Control Design," *AIAA Guidance, Navigation, and Control Conference*, AIAA 2002-5055, 2002.

[30] Calise, A. J., Yang, B., and Craig, J. I., "Augmenting Adaptive Control Approach to Control of Flexible Systems," *Journal of Guidance, Control, and Dynamics*, Vol. 27, No. 3, 2001, pp. 387–396.